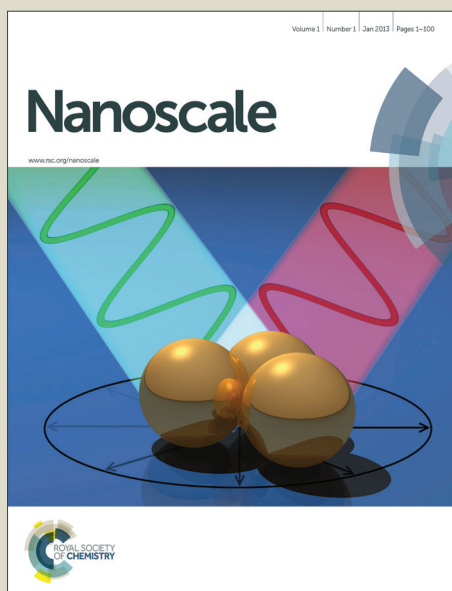


Nanoscale

Accepted Manuscript



This is an *Accepted Manuscript*, which has been through the Royal Society of Chemistry peer review process and has been accepted for publication.

Accepted Manuscripts are published online shortly after acceptance, before technical editing, formatting and proof reading. Using this free service, authors can make their results available to the community, in citable form, before we publish the edited article. We will replace this *Accepted Manuscript* with the edited and formatted *Advance Article* as soon as it is available.

You can find more information about *Accepted Manuscripts* in the [Information for Authors](#).

Please note that technical editing may introduce minor changes to the text and/or graphics, which may alter content. The journal's standard [Terms & Conditions](#) and the [Ethical guidelines](#) still apply. In no event shall the Royal Society of Chemistry be held responsible for any errors or omissions in this *Accepted Manuscript* or any consequences arising from the use of any information it contains.

ARTICLE

Oxidized/reduced graphene nanoribbons facilitate charge transfer to the $\text{Fe}(\text{CN})_6^{3-}/\text{Fe}(\text{CN})_6^{4-}$ redox couple and towards oxygen reduction

Cite this: DOI: 10.1039/x0xx00000x

Fábio de Lima and Gilberto Maia*

Received 00th January 2012,
Accepted 00th January 2012

DOI: 10.1039/x0xx00000x

www.rsc.org/

This study investigated the synthesis of graphene oxide nanoribbons (GONRs) and graphene nanoribbons (GNRs) from multiwalled carbon nanotubes (MWCNTs), and the behavior of thin films of MWCNTs, GONRs, and GNRs on a glassy carbon surface in the presence of two redox probes ($\text{Fe}(\text{CN})_6^{3-}/\text{Fe}(\text{CN})_6^{4-}$ and O_2) employing cyclic voltammetry, electrochemical impedance spectroscopy, and hydrodynamic voltammetry (HV) as a simple procedure for characterizing these films. The feasibility of using these electrochemical techniques to this end opens up the possibility of applying them to biosensors and electrocatalysts using surface-supported MWCNT, GONR, and GNR materials. GNR1 resembles an internodal segment of bamboo cut lengthwise, with a shallow troughing at its center, while GNR2 resembles stacked ribbons, each ~16 nm wide, with points of structural damage and points of four-ribbon connection measuring 60 nm or wider, sufficiently catalytic for the oxygen reduction reaction to occur, unlike the other modified electrodes investigated in acidic, 0.1 M KH_2PO_4 (pH 7.0), and 0.1 M KOH solutions (HV results). Transmission electron microscopy and thermogravimetric analysis were employed to characterize the MWCNTs, GONRs, and GNRs.

Introduction

Carbon nanomaterials, such as N-doped nanotubes, graphene, and mesoporous carbon,¹ have been extensively studied in a wide range of fields (*e.g.*, adsorption,² catalysis,³ and sensor technology²), owing to their unparalleled good electrical conductivity and high surface area, in addition to superior electrocatalytic activity towards the oxygen reduction reaction (ORR).¹

The Tour group⁴ obtained oxidized nanoribbons—thin, elongated strips of graphene (GN) that have straight edges, termed graphene oxide nanoribbons (GONRs)⁵—by suspending multiwalled carbon nanotubes (MWCNTs) for 1–12 h in concentrated sulfuric acid, followed by treatment with 5 times KMnO_4 wt. in relation to MWCNTs wt. for 1 h at room temperature and 1 h at 55–70 °C. These nanotubes appeared to open along a line, similarly to the “unzipping” of graphite oxide^{6,7}—a mechanism explained in terms of oxidation of alkenes by permanganate in acid,⁸ as supported by theoretical calculations.⁹ These GONRs were reduced with 1 vol% concentrated ammonium hydroxide and 1 vol% hydrazine monohydrate,⁴ yielding GN strips with high length-to-width ratios and straight edges, termed graphene nanoribbons (GNRs),^{5,10} which change from being semiconductors to semimetals as their width is increased,¹⁰ in a process that chemically unzips the nanotubes, forming nanoribbons up to 4 μm long, 100–500 nm wide, and 1–30 GN layers thick.¹¹

The Tour group⁴ also performed the same unzipping process in single-walled carbon nanotubes (SWCNTs), producing narrow nanoribbons more resistant to disentanglement. They also reported⁵ variations in the conditions required for GONR synthesis, including availability of sufficient H_2SO_4 (~90 vol%) for complete formation and exfoliation of the nanoribbons, relatively high temperatures (60

°C), and addition of a second acid ($\text{C}_2\text{HF}_3\text{O}_2$ or H_3PO_4 , 10 vol%) to $\text{H}_2\text{SO}_4/\text{KMnO}_4$ ^{5,8}—in contrast with their previous study⁴—and claimed to have produced novel nanoribbons with a higher degree of oxidation (by *in situ* protection of the vicinal diols formed on the basal plane of graphene during oxidation, thereby preventing their overoxidation to diones), but lower formation of holes bearing carbonyl and carboxyl moieties.⁵ Electrical measurements of the ribbon devices revealed that optimized hydrazine-reduced GNRs were 2–20 times more conductive than unoptimized hydrazine-reduced GNRs.⁵

Jiao *et al.*¹² performed controlled unzipping of MWCNTs to produce GNRs by Ar plasma etching of nanotubes partly embedded in a polymer film—the film was subsequently removed using solvent vapor, and the resulting nanoribbons were heated at 300 °C to remove any residual polymer¹¹—or by using raw soot material containing pristine MWCNTs synthesized by arc-discharge previously calcined in air at 500 °C (to remove impurities and etch/oxidize MWCNTs at defect sites and ends) and dispersed in a 1,2-dichloroethane (DCE) organic solution of poly(*m*-phenylenevinylene-co-2,5-dioctoxy-*p*-phenylenevinylene) (PmPV) by sonication.¹³

Dai and co-workers,¹⁴ using their approach of sonochemically unzipping MWCNTs grown by arc-discharge in an organic polymer solution¹⁴ to produce ~10–30 nm-wide GNRs, found a high percentage of two-layer GNRs and some single-layer ribbons, with layer–layer stacking angles ranging from 0° to 30° and average chiral angles of around 30° (armchair orientation) or 0° (zigzag orientation), in addition to a large proportion of GNRs with bent and smooth edges, while the remainder exhibited flat, less smooth edges (roughness ≤1 nm). They also produced GNRs by exfoliating commercial expandable graphite (made by intercalating ~350 μm–

scale graphite flakes with sulfuric acid and nitric acid) by briefly (60 s) heating them to 1000 °C in forming gas (3% hydrogen in argon), sonicating the resulting exfoliated material in a DCE solution of PmPV, and centrifuging the suspension to retain the GNRs (together with small sheets) in the supernatant (only ~0.5% of the starting material was retained).¹⁵ (See also other unzipping nanotube processes classified by Terrones.⁸)

Envisaged uses of GNRs produced by unzipping carbon nanotubes include construction of robust polymer composites, biosensors, chemical sensors, catalysts, electronic devices, conductive paints, scaffolds for tissue regeneration, and drug delivery agents.^{8,11}

Dai and co-workers¹⁶ showed that few-walled carbon nanotubes, following outer wall exfoliation via oxidation and high-temperature reaction with ammonia, acted as an ORR electrocatalyst in both acidic and alkaline solutions. In their experiment, the outer walls of few-walled carbon nanotubes were partially unzipped under oxidative conditions, creating nanoscale sheets of graphene attached to the inner tubes—*i.e.*, few-walled carbon nanotube-graphene (NT-G) complexes, which contained small amounts of iron, originating from nanotube growth seeds, and nitrogen impurities, resulting in the formation of catalytic sites that improved catalytic activity. The investigators hypothesized that the high degree of carbon nanotube graphitization, the exfoliated outer walls, and the graphene pieces in the NT-G sample might be responsible for imparting high oxidative corrosion resistance to the catalytic sites and thereby high durability to the NT-G ORR electrocatalyst.

Gong *et al.*¹⁷ found that vertically aligned nitrogen-containing carbon nanotubes (VA-NCNTs) can act as effective metal-free ORR electrocatalysts even after complete removal of the residual Fe catalyst by electrochemical purification, suggesting that the ORR activity of VA-NCNTs is solely due to nitrogen doping.¹⁸ In alkaline electrolytes, these metal-free VA-NCNTs have been shown to catalyze a four-electron ORR process with much higher catalytic activity, lower overpotential, smaller crossover effect, and better long-term operation stability, compared with commercially available Pt/carbon black catalysts (C2-20, 20% platinum on Vulcan XC-72R; E-Tek).^{17,18} Yang *et al.*¹⁹ developed a metal-free electrocatalyst of boron-doped carbon nanotubes that exhibited good performance in ORR in terms of electrocatalytic activity, stability, and immunity to methanol crossover and CO poisoning. Electrocatalytic performances were progressively improved by increasing boron content, as reflected in the increased reduction current and the positively shifted onset and peak potentials.

Park *et al.*²⁰ reported that a series of nitrogen-doped reduced graphene oxide (NRGO_n) nanosheets (starting with graphite powder and prepared through covalent functionalization using various small organic molecules and a subsequent thermal treatment) exhibited varying degrees and configurations of nitrogen atoms within the graphitic framework, depending on the type of precursors employed. NRGO3, with a high degree of pyridinic N content, displayed a one-step, quasi-four-electron transfer pathway during ORR, similarly to commercial Pt/C. Yamauchi and co-workers¹ reported that highly N-doped mesoporous carbon spheres (NMCSSs) with extra-large mesopores (up to 16 nm), obtained through self-polymerization of dopamine (DA) and spontaneous co-assembly of diblock copolymer micelles, showed high electrocatalytic activity and excellent long-term stability towards ORR, even comparable to those exhibited by a Pt/C catalyst.

Huang *et al.*²¹ produced multilayer films containing electrochemically reduced graphene oxide (ERGO) using an alternating layer-by-layer assembly of negatively charged graphene oxide (GO, synthesized from graphite powder) and positively charged poly(diallyldimethylammonium chloride) (PDDA), in

combination with an electrochemical reduction procedure. As a metal-free catalyst, the resulting [PDDA@ERGO] multilayer film showed electrocatalytic activity towards ORR, with methanol tolerance in alkaline media.

Based on knowledge of synthetic routes to produce GONRs and GNRs (including ~10–30 nm-wide GNRs) from unzipping MWCNTs, and considering that GNRs can act as catalysts, while VA-NCNTs, NRGO_n, and ERGO can act as electrocatalysts, towards ORR, the primary purpose of the present study was to synthesize GONRs and GNRs from MWCNTs and employ cyclic voltammetry (CV), electrochemical impedance spectroscopy (EIS), and hydrodynamic voltammetry (HV) as a simple characterizing procedure to investigate the behavior of thin films of MWCNTs, GONRs, and GNRs on a glassy carbon (GC) surface in the presence of two redox probes: Fe(CN)₆^{3-/4-} and O₂. This allowed differences in the behavior of these modified electrodes to be identified and explained—information that can lead to the use of these detection tools in biosensors and electrocatalysts based on MWCNT, GONR, and GNR materials. Transmission electron microscopy (TEM) and thermogravimetric (TG) analysis were employed to characterize MWCNTs, GONRs, and GNRs.

Results and Discussion

Comparison of MWCNT1, MWCNT2, GONR1, GONR2, GNR1, and GNR2 structures

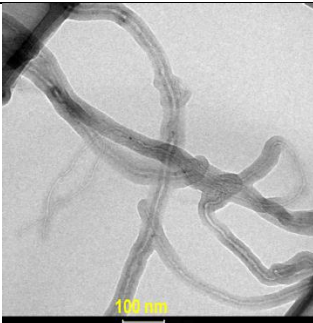
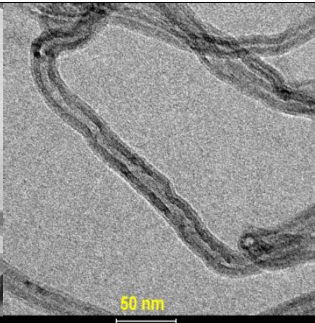
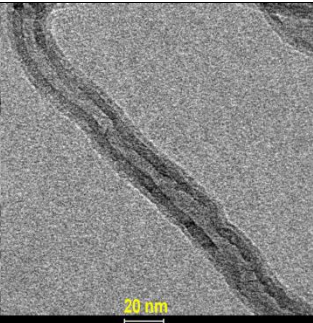
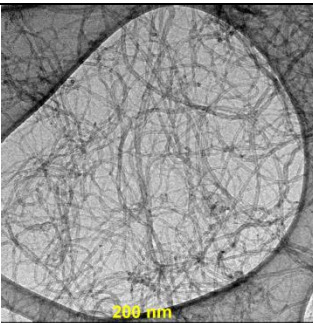
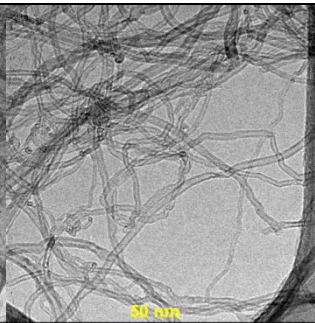
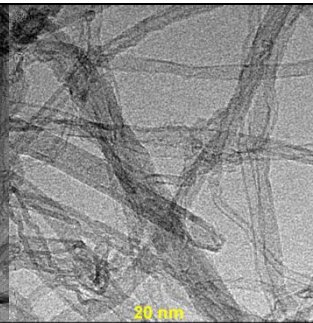
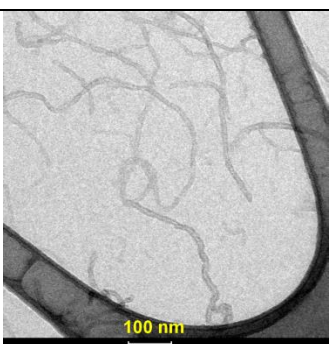
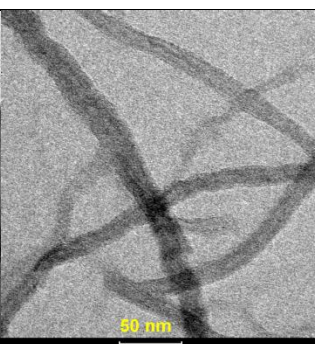
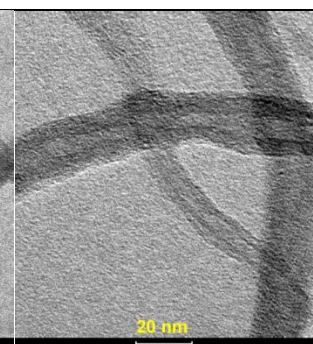
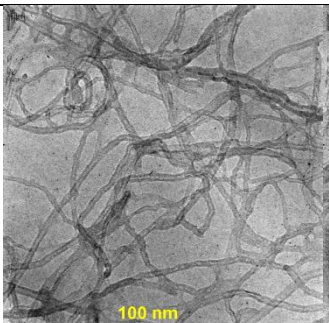
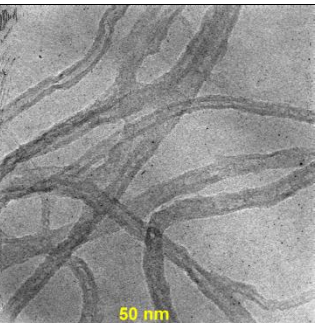
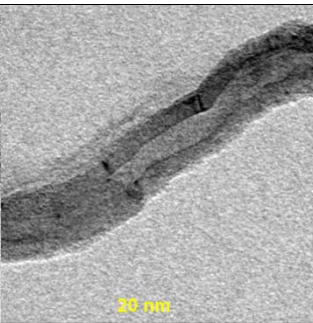
Our method for synthesizing GNR1 and GNR2, by reduction of GONR1 and GONR2 with hydrazine,^{22,23} was the same technique used by the Tour group,⁴ while our method for producing GONR1 and GONR2 differed.^{4,5,8,10,11} The Tour group⁵ produced GONRs with sufficient H₂SO₄ (~90 vol%) at relatively high temperatures (60 °C) and used a second acid (C₂H₅F₃O₂ or H₃PO₄, 10 vol %), added to H₂SO₄/KMnO₄.^{5,8}

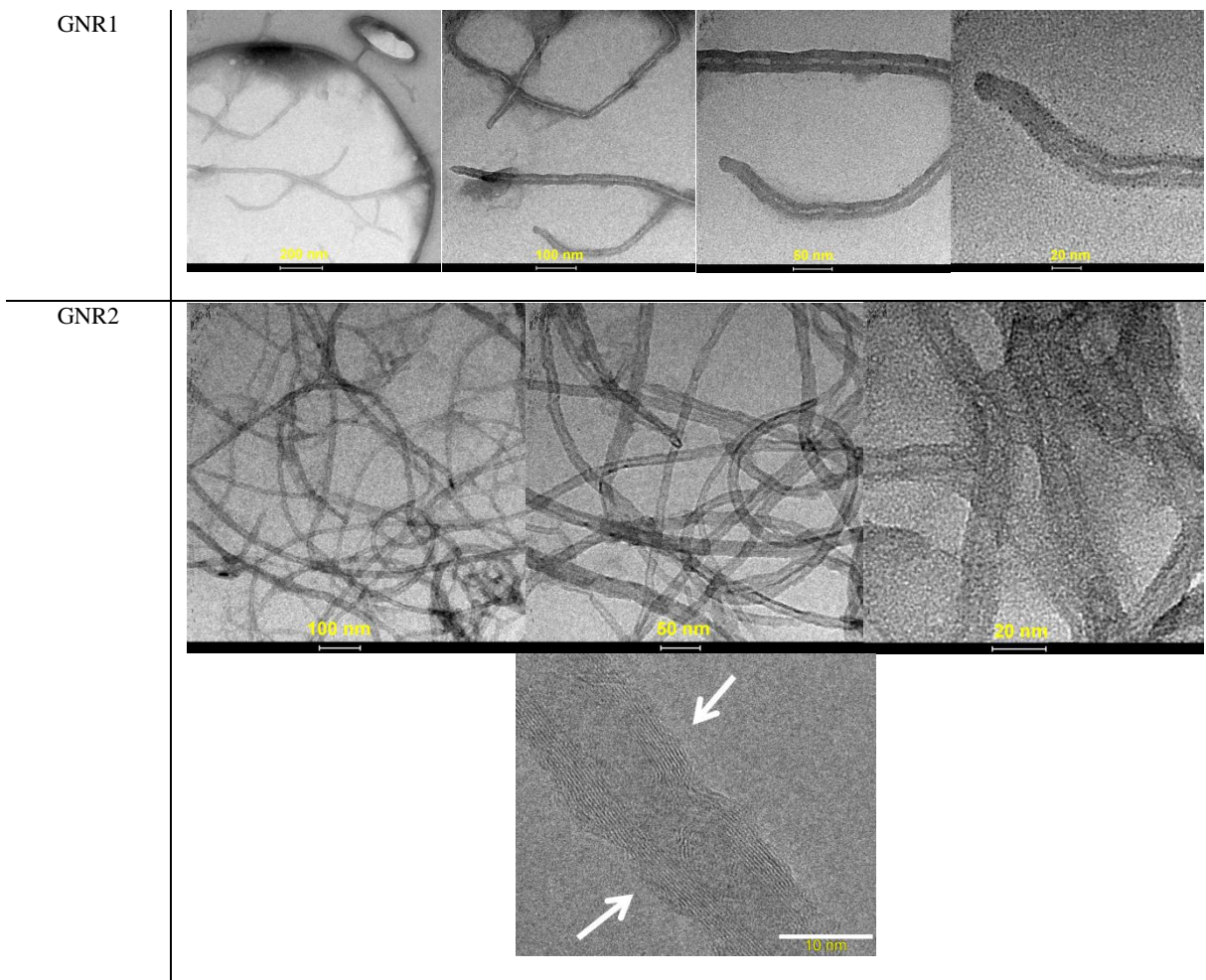
Table 1 depicts TEM images of our synthesized compounds. As seen in Table 1, MWCNT1 and MWCNT2 exhibit bamboo-like compartments characteristic of MWCNTs.²⁴ MWCNT1, with a diameter in the range of 5 to 20 nm, has more compact walls and a hollow center, whereas MWCNT2 exhibits concentric hollow tubes with diameters in the range of 5 to 20 nm. The central hollows are virtually absent from GONR1 and GONR2 and these carbon nanostructures measure around 20 nm across after MWCNT1 and MWCNT2 have undergone oxidation steps (an uncommon feature, since it is assumed that GONRs wider than 100 nm are most likely oxidatively consumed during the oxidation process,^{4,5} while it has been shown that MWCNTs under 50 nm across are not unzipped,²⁴ and 10-to-30 nm-wide GNRs have been generated using sonochemical unzipping of MWCNTs¹⁴). In addition, GONR1 and GONR2 are mainly constituted of stacked ribbons and a few exfoliated ribbons (Table 1), features that are indicative of pronounced oxidation,^{4,24} starting from the open ends and, after unzipping, continuing from the edges and advancing towards the middle of the unzipping nanotube.²⁴ GNR1 resembles an internodal segment of bamboo cut lengthwise, with a shallow troughing at its center, while GNR2 resembles stacked ribbons, each ~16 nm wide—similar to the product obtained by moderate reduction with hydrazine²⁴—with points of structural damage and points of four-ribbon connection measuring 60 nm or wider (Table 1).

The high-resolution TEM (HRTEM) image of GNR2 (Table 1) clearly shows a nanometer-sized graphene membrane pattern²⁵ (indicated by arrows) at the edges of the GNR2 structure. Because electron contrast depends on the angle of incidence, the graphene membrane pattern is not seen over the entire image. This HRTEM image of the pattern is similar to the HRTEM image of nanometer-sized graphitic sheets obtained by Yamauchi and co-workers,²

suggesting that the original sp^2 -bonded carbon atoms are retained and/or restored after GONR2 reduction with aqueous hydrazine sulfate (see Experimental Section).

Table 1. Representative TEM images of MWCNT1, MWCNT2, GONR1, GONR2, GNR1, and GNR2 structures.

Material	TEM		
MWCNT1			
MWCNT2			
GONR1			
GONR2			



TG Analysis of MWCNT1, MWCNT2, GONR1, GONR2, GNR1, and GNR2

The TG thermograms in Figure 1 reveal mass loss as a function of temperature for MWCNT1, MWCNT2, GONR1, GONR2, GNR1, and GNR2.

As depicted in Figure 1, MWCNT1 and MWCNT2 underwent mass loss (~13%) above 500 °C. GONR1 and GONR2 started to lose mass (~10%) even earlier, below 100 °C, a behavior that can be ascribed to removal of adsorbed water.^{22,26} Mass losses were also observed at ~175 and 252 °C (~15% in total), presumably due to pyrolysis of labile oxygen-containing functional groups, yielding CO, CO₂, and water vapor.^{22,26-28} Linear mass loss occurred above 252 °C (~22% for GONR1 and 16% for GONR2), characterizing the presence of more stable oxygen functionalities and an end material considerably more unstable than the initial material, and revealing GONR2 to be more stable (low mass loss) than GONR1, consistent with the presence of a more packaged structure (see the GONR1 TEM image in Table 1) that possibly has more oxygen-containing functional groups at its edge than does GONR2.

On the other hand, GNR2 proved more stable than both GNR1 and GNR02, while GNR1 was more stable than GONR1, due to a decrease in thermally labile oxygen functional groups (deoxygenation)^{22,28} by chemical reduction with hydrazine. Apart from linear mass loss (~11%) observed up until ~500 °C (Figure 1), suggesting that the labile oxygen functional groups in GNR2 were largely removed by reacting with hydrazine,^{22,26} GNR2 subsequently underwent no more than ~18% mass loss until ~900 °C, implying

that oxygen functionalities of higher stability are not completely eliminated from GNR2 by chemical reduction.^{22,26,27,29} GNR1 underwent linear mass loss (~16%) up until ~500 °C (Figure 1), suggesting the presence of a greater amount of labile oxygen functional groups (more eroded surface, Table 1) than in GNR2, and roughly the same amount of stable oxygen functionalities, not completely eliminated from GNR1 by chemical reduction.^{22,26,27,29} For MWCNT1, MWCNT2, GNR1, and GNR2, mass losses differed from published data for graphite (GR) and chemically converted graphene (CCG).²²

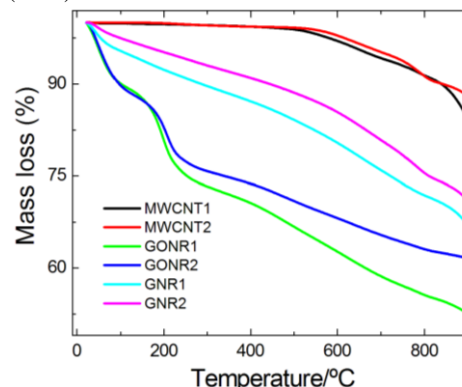


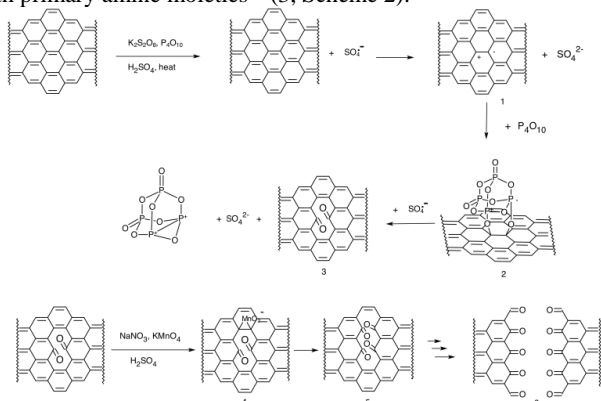
Figure 1. Decomposition behavior of MWCNT1, MWCNT2, GONR1, GONR2, GNR1, and GNR2.

Probable mechanism of GONR1 or GONR2 synthesis from MWCNT1 or MWCNT2, and GNR1 or GNR2 from GONR1 or GONR2

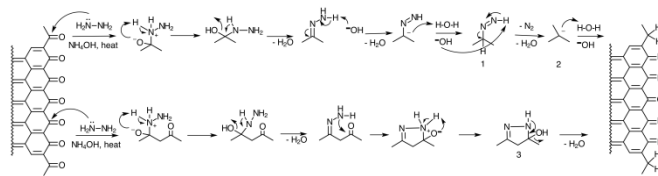
During the pre-oxidation step, the mechanism of MWCNT1 and MWCNT2 unzipping can be assumed as akin to that report for the oxidation of aromatic substrates (also applicable to olefins) by peroxydisulfate ($\text{S}_2\text{O}_8^{2-}$), thought to occur via an electron-transfer mechanism involving a sulfate radical anion ($\text{SO}_4^{\cdot-}$) that can be generated in the reaction medium by thermal heating³⁰ (1, Scheme 1). This is followed by formation of phosphorus pentoxide ester (2, Scheme 1) and by a second oxidation with $\text{SO}_4^{\cdot-}$, made possible by a juxtaposition of buttressing ketones, which distorts β,γ -alkenes, rendering them more susceptible to a new subsequent attack by $\text{SO}_4^{\cdot-}$, yielding a dione (3, Scheme 1). Oxidation then proceeds as described for the oxidation of alkenes by permanganate in acid.⁴ The proposed first step in the process involves manganese ester formation (4, Scheme 1) and further oxidation facilitated by juxtaposition of buttressing ketones, which distorts β,γ -alkenes, rendering them more susceptible to a subsequent attack by permanganate, yielding a dione (5, Scheme 1) in the dehydrating medium^{4,31} (acid and NO_3^-).

As the process advances, the buttressing-induced strain on β,γ -alkenes lessens, for lack of space for carbonyl projection, although bond-angle strain induced by the enlarging hole (or tear, if originating from the end of the nanotube) would make β,γ -alkenes (5, Scheme 1) increasingly reactive.⁴ Hence, once unzipping has been initiated, its further development is enhanced, relative to an unzipped tube or to an as yet unengaged site on the same tube.⁴ Finally, relief of the bond-angle strain when the nanotube opens to the graphene ribbon (6, Scheme 1) slows further dione formation and cutting.^{4,31} Thus, the preference for sequential bond cleavage over random opening and subsequent cutting can be explained by a concerted attachment to neighboring carbon atoms, initially by phosphorus pentoxide during pre-oxidation, followed by permanganate in the proceeding oxidation step. The surface of the now less strained nanoribbon remains prone to 1,2-diol formation, which leads to overall high oxidation of the ribbon, but is less likely to result in further oxidative cutting, yielding the dione, owing to relief of the tubular strain on the double bonds.⁴

A mechanism for GONR1 and GONR2 hydrazine reduction to produce GNR1 and GNR2, respectively, is proposed in Scheme 2. Park *et al.*³² suggested that hydrazone groups are generated in situations where non-aromatic $\text{C}=\text{N}$ double bonds result from the reaction between hydrazines and ketones or aldehydes^{33,34} (1, Scheme 2). In alkaline media, however, hydrazine can convert a ketone group into a methylene group—a mechanism also known as Wolff–Kishner reduction³⁴ (2, Scheme 2). Park *et al.*³² also proposed that pyrazole groups can be produced by reacting diketone groups with primary amine moieties³⁵ (3, Scheme 2).



Scheme 1. Proposed mechanism for production of GONR1 and GONR2 from MWCNT1 and MWCNT2, respectively.



Scheme 2. Proposed mechanism for production of GNR1 and GNR2 from GONR1 and GONR2, respectively.

CV responses provided by bare CG electrode and GC electrodes modified with MWCNT1, MWCNT2, GONR1, GONR2, GNR1, or GNR2 at different loadings, in an N_2 -saturated 0.1 M KCl solution concomitantly with a total 2 mM concentration of $\text{K}_3[\text{Fe}(\text{CN})_6]/\text{K}_4[\text{Fe}(\text{CN})_6]$ (1:1 molar ratio) or otherwise

Figure 2 shows the CV responses of a bare GC electrode and GC electrodes surface-modified with $80 \mu\text{g cm}^{-2}$ of MWCNT2, GONR2, or GNR2 (termed GC/MWCNT2, GC/GONR2, and GC/GNR2, respectively) obtained in an N_2 -saturated 0.1 M KCl solution concomitantly with a total 2 mM concentration of $\text{K}_3[\text{Fe}(\text{CN})_6]/\text{K}_4[\text{Fe}(\text{CN})_6]$ (1:1 molar ratio) or otherwise. The current densities shown in Figure 2 were obtained by dividing the currents by ECSA values.²²

CV responses obtained in N_2 -saturated 0.1 M KCl for bare GC and GC electrodes surface-modified with $80 \mu\text{g cm}^{-2}$ of MWCNT2, GONR2, or GNR2 (Figure 2) comprised solely capacitive current densities (with an absence of faradaic peaks or current densities) for bare GC, which were amplified when the GC/MWCNT2 electrode was employed, owing to the highly porous MWCNT2 layer formed onto the GC surface (Figure 2, black and red curves, respectively). For GC modified with $80 \mu\text{g cm}^{-2}$ of GONR2 or GNR2 (Figure 2, green and blue curves, respectively), large capacitive current densities can be observed, characteristic of the ability of graphene electrodes (as is the case with GNR2) to act as electric double-layer capacitors (DLCs, also termed supercapacitors or ultracapacitors), storing charge in the double layer formed at an electrolyte–electrode interface when a potential is applied.^{22,23,36–39} Also, a small redox couple is seen at around 0.0 V, characteristic of oxidation/reduction of quinones remaining on the graphene surface, and is highly enhanced for the GC/GONR2 electrode (Figure 2, green curve).

In the presence of a total 2 mM concentration of $\text{K}_3[\text{Fe}(\text{CN})_6]/\text{K}_4[\text{Fe}(\text{CN})_6]$ (1:1 molar ratio), however, a characteristic $\text{Fe}(\text{CN})_6^{3-}/\text{Fe}(\text{CN})_6^{4-}$ redox behavior is observed for bare GC and modified GC electrodes²² (Figure 2), with redox peaks centered at 0.17 V and an $I_p(\text{anodic})/I_p(\text{cathodic})$ ratio of 1. Note that in the presence of $\text{Fe}(\text{CN})_6^{3-}/\text{Fe}(\text{CN})_6^{4-}$ redox probes, current densities are higher for GC/GNR2 than for bare GC, GC/MWCNT2, or GC/GONR2. Peak potential separation approached 78, 102, 63, and 84 mV for bare GC, GC/MWCNT2, GC/GONR2, and GC/GNR2, respectively (Figure 2), enhancing the surface effect that modified GC electrodes had on $\text{Fe}(\text{CN})_6^{3-}/\text{Fe}(\text{CN})_6^{4-}$ redox behavior, since the only difference between bare and modified GC electrodes (Figure 2) was the presence of a surface film containing $80 \mu\text{g cm}^{-2}$ of MWCNT2, GONR2, or GNR2 (see also Figures S1–S7, Supporting Information, for a more detailed comparison of CV results for different potential scan rates and different modified GC electrodes). ECSA increased from 0.33 cm^2 for bare GC to 0.37, 0.64, and 0.77 cm^2 for GC/MWCNT2, GC/GONR2, and GC/GNR2, respectively (see Table S1, Supporting Information), while the opposite behavior was observed for GR, GO, and CCG by Lima and co-workers.²² Also, the current densities shown in Figure 2 are five times lower than that obtained by Lima and co-workers,²² who employed a five times higher concentration of $\text{K}_3[\text{Fe}(\text{CN})_6]/\text{K}_4[\text{Fe}(\text{CN})_6]$.

Figure 3 depicts the behavior of $\text{Fe}(\text{CN})_6^{3-}/\text{Fe}(\text{CN})_6^{4-}$ redox probes on GC/GONR2 and GC/GNR1 electrodes prepared with different loadings of surface modifier.

Although CV responses are similar to those described in Figure 2, current densities diminish with decreasing loadings of surface modifier onto the GC surface (approaching the behavior of bare GC—see black line, Figure 3). High current densities follow the behavior of high capacitive current densities, the magnitude of which can be attributed to the large loading of modifier present on the GC surface in the absence of $\text{Fe(CN)}_6^{3-}/\text{Fe(CN)}_6^{4-}$ redox probes. The sharp changes in current density observed at both potential boundaries for the CV curves corresponding to GC/GNR2 and GC/GNR1 (see also Figure 2 and Figures S6 and S7 in Supporting Information) are explained by the ability of these electrodes to act as electric DLCs, storing charge in the double layer formed at an electrolyte–electrode interface when a potential is applied.^{22,23,36–39}

Also, when the potential scan rate is increased (see Figures S6 and S7, the Supporting Information), CV curves remain rectangular in shape at both potential boundaries, confirming the formation of efficient DLCs and fast charge propagations within the GNR2 and GNR1 layers for loadings of 80 (predominantly), 32, or 8 $\mu\text{g cm}^{-2}$ onto the GC/GNR2 and GC/GNR1 electrodes.^{22,23,36,39} Peak potential separation approached 75, 71, and 60 mV for GC/GNR2 electrodes (Figure 3A), and 86, 86, and 74 mV for GC/GNR1 electrodes (Figure 3B). *EC*SA rises from 0.38 to 0.43 cm^2 for GC/GNR2 electrodes, and from 0.36 to 0.47 cm^2 for GC/GNR1 electrodes, as the loading of surface modifier is increased (see Table S1, the Supporting Information). A similar behavior has been reported for GC/CCG electrodes.²²

EIS responses provided by bare GC electrode and GC electrodes modified with MWCNT1, MWCNT2, GONR1, GONR2, GNR1, or GNR2 at different loadings, in an N_2 -saturated 0.1 M KCl solution concomitantly with a total 2 mM concentration of $\text{K}_3[\text{Fe(CN)}_6]/\text{K}_4[\text{Fe(CN)}_6]$ (1:1 molar ratio)

In order to elucidate the electrochemical responses depicted in Figures 2, 3, and S1–S7 (Supporting Information), EIS experiments were conducted at OCP, which measured 0.19 V on average for bare and modified GC electrodes in the presence of a total 2 mM concentration of $\text{K}_3[\text{Fe(CN)}_6]/\text{K}_4[\text{Fe(CN)}_6]$ (1:1 molar ratio) (Figure 4).

Figure 4 shows typical EIS results for complex-plane impedance plots combining regions of mass transfer and kinetic control at low and high frequencies, respectively.⁴⁰ When the electrochemical system is kinetically sluggish, large R_{ct} values (charge transfer resistance) are found within a well-defined semicircular region, displaying a limited frequency range in which mass transfer is a significant factor.⁴⁰ When R_{ct} is small, the system is so kinetically facile that mass transfer always plays a role and the semicircular region is not well defined⁴⁰ (Figure 4).

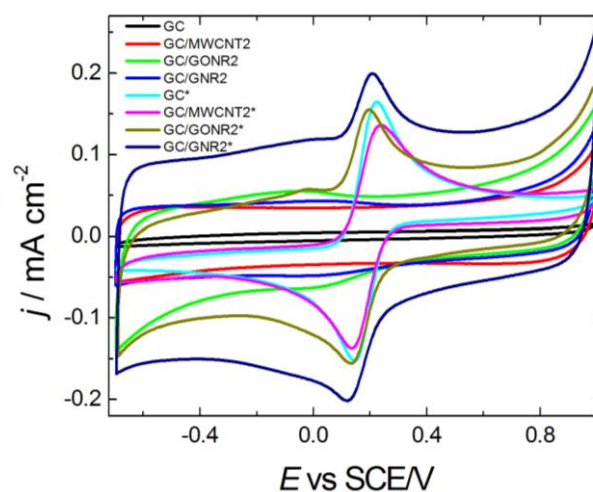


Figure 2. Cyclic voltammograms obtained in N_2 -saturated 0.1 M KCl with a bare GC electrode and GC electrodes surface-modified with 80 $\mu\text{g cm}^{-2}$ of MWCNT2, GONR2, or GNR2 (termed GC, GC/MWCNT2, GC/GONR2, and GC/GNR2, respectively) and in N_2 -saturated 0.1 M KCl containing a total 2 mM concentration of $\text{K}_3[\text{Fe(CN)}_6]/\text{K}_4[\text{Fe(CN)}_6]$ (1:1 molar ratio) for a bare GC electrode and GC electrodes surface-modified with 80 $\mu\text{g cm}^{-2}$ of MWCNT2, GONR2, or GNR2 (termed GC*, GC/MWCNT2*, GC/GONR2*, and GC/GNR2*, respectively). Room temperature; $\nu = 50 \text{ mV s}^{-1}$. Scans started at 1.0 V.

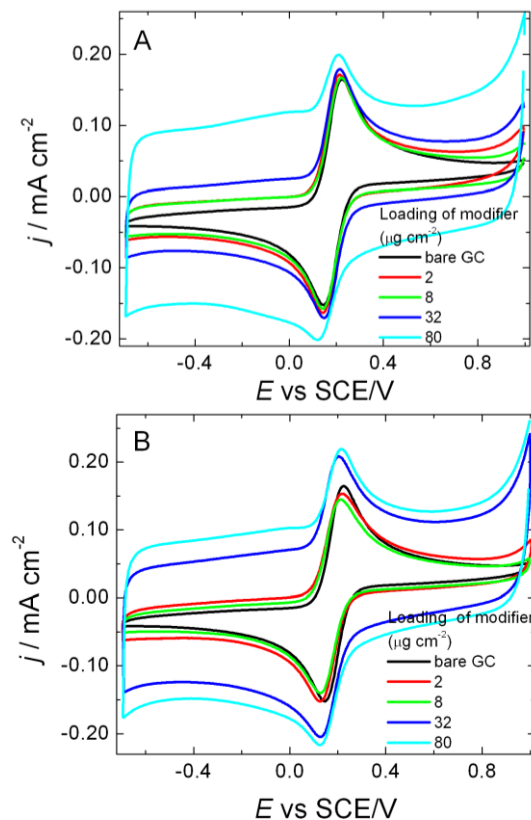


Figure 3. Cyclic voltammograms obtained in N_2 -saturated 0.1 M KCl containing a total 2 mM concentration of $\text{K}_3[\text{Fe(CN)}_6]/\text{K}_4[\text{Fe(CN)}_6]$ (1:1 molar ratio) for a bare GC electrode and GC electrodes surface-modified with (A) GNR2 and (B) GNR1. Room temperature; $\nu = 50 \text{ mV s}^{-1}$. Scans started at 1.0 V.

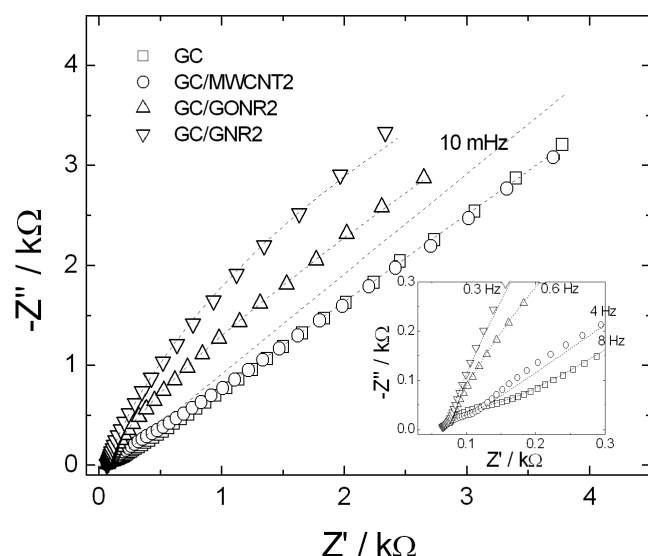
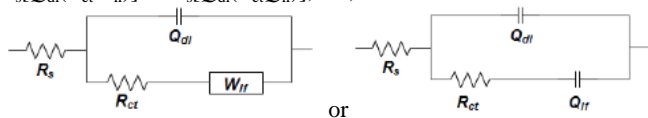


Figure 4. Plane impedance plots obtained in an N_2 -saturated 0.1 M KCl solution containing a total 2 mM concentration of $K_3[Fe(CN)_6]/K_4[Fe(CN)_6]$ (1:1 molar ratio) for a bare GC electrode (\square) and GC electrodes surface-modified with $80 \mu g cm^{-2}$ of MWCNT2 (\circ), GONR2 (\triangle), or GNR2 (∇). Potential perturbation: 25 mV (rms). Frequency range: 100 kHz–10 mHz. Constant potential for EIS acquisition: OCP (0.19 V vs. SCE on average). Lines represent spectra (adjusted) calculated using a non-linear least-squares program, conforming to the equivalent circuit $R_s[Q_{dl}(R_{ct}W_{lf})]$, or $R_s[Q_{dl}(R_{ct}Q_{lf})]$. Calculated average values: $R_s = 70 \Omega$, $Q_{dl} = 0.42 mF s^{n-1}$, $n = 0.5$, $W_{lf} = 0.6 mF$. Inset: Impedance plane plots restricted to 0.3 k Ω in the main graph.

The simplest equivalent circuit of an electrochemical cell is a Randles equivalent circuit composed of resistors and capacitors.⁴⁰ This type of equivalent circuit was used in the present study and perfectly fitted the EIS results obtained (lines on the EIS curves shown). The equivalent circuit employed can be represented as $R_s[Q_{dl}(R_{ct}W_{lf})]$ or $R_s[Q_{dl}(R_{ct}Q_{lf})]$, i.e.,



respectively, where R_s stands for the solution resistance, Q_{dl} for the constant phase element involving an n exponent to represent C_{dl} , W_{lf} for a Warburg impedance indicating a purely diffusion-controlled process at the low-frequency limits,⁴¹ and Q_{lf} stands for a constant-phase element at the low-frequency limits.

The results obtained at OCP (Table 1) revealed k^0 to be lower ($0.01250 cm s^{-1}$) for bare GC in the presence of a total 2 mM concentration of $K_3[Fe(CN)_6]/K_4[Fe(CN)_6]$ (1:1 molar ratio) than for GC modified with $32 \mu g cm^{-2}$ of MWCNT1 or modified with $80 \mu g cm^{-2}$ of MWCNT2 or GONR2, or (with the highest k_{app}^0 value, approaching $0.02065 cm s^{-1}$) with $80 \mu g cm^{-2}$ of GNR1. The presence of $32 \mu g cm^{-2}$ of GNR2 on the GC surface is sufficient to produce a high k_{app}^0 value (see Figure 4 and Table 1). (See Lima et al.²² for the conditions adopted for EIS measurements. Briefly, k_0 (the standard heterogeneous rate constant) (or k_{app}^0) = $RT/F^2R_{ct}(ECSCA)C$ (for single-electron transfers), where R is the universal gas constant, T is the absolute temperature, n is the number of electrons involved in an electrode reaction, F is the Faraday constant, and C is the species concentration in the solution.) When the loading of modifiers present on GC was decreased (Table 1) to 32, 8, and $2 \mu g cm^{-2}$, the corresponding charge transfer rates

calculated were 29, 31, and 24 times lower (with k_{app}^0 approaching 0.00043 , 0.00040 , and $0.00052 cm s^{-1}$, respectively; Table 1) than for bare GC, and the modified surfaces thus prepared proved capable of sufficiently decreasing charge transfer to the $Fe(CN)_6^{3-}/Fe(CN)_6^{4-}$ probes at OCP.

Table 1 Approximate R_{ct} and k^0 (or k_{app}^0) values obtained from non-linear least-squares calculations for elements of the equivalent circuit $R_s[Q_{dl}(R_{ct}W_{lf})]$, or $R_s[Q_{dl}(R_{ct}Q_{lf})]$, adjusted for EIS responses (for example, see Figure 4 and Figure S8, Supporting Information) obtained in a N_2 -saturated 0.1 M KCl solution containing a total 2 mM concentration of $K_3[Fe(CN)_6]/K_4[Fe(CN)_6]$ (1:1 molar ratio) using a bare GC electrode and GC electrodes surface-modified with different loadings of MWCNT1, MWCNT2, GONR1, GONR2, GNR1, or GNR2.

Electrode (and modifier loading)	R_{ct}/Ω	k^0 (or k_{app}^0)/ $cm s^{-1} \times 10^5$ [a]
Bare GC	65	1250
GC/MWCNT2 ($80 \mu g cm^{-2}$)	27	2634
GC/MWCNT2 ($32 \mu g cm^{-2}$)	1016	114
GC/MWCNT2 ($8 \mu g cm^{-2}$)	7981	40
GC/MWCNT2 ($2 \mu g cm^{-2}$)	3757	52
GC/MWCNT1 ($80 \mu g cm^{-2}$)	35	1536
GC/MWCNT1 ($32 \mu g cm^{-2}$)	38	1644
GC/MWCNT1 ($8 \mu g cm^{-2}$)	412	291
GC/MWCNT1 ($2 \mu g cm^{-2}$)	182	611
GC/GONR2 ($80 \mu g cm^{-2}$)	18	2297
GC/GONR2 ($32 \mu g cm^{-2}$)	1132	43
GC/GONR2 ($8 \mu g cm^{-2}$)	90	812
GC/GONR2 ($2 \mu g cm^{-2}$)	90	815
GC/GONR1 ($80 \mu g cm^{-2}$)	369	244
GC/GONR1 ($32 \mu g cm^{-2}$)	413	262
GC/GONR1 ($8 \mu g cm^{-2}$)	170	414
GC/GONR1 ($2 \mu g cm^{-2}$)	2045	59
GC/GNR2 ($80 \mu g cm^{-2}$)	83	416
GC/GNR2 ($32 \mu g cm^{-2}$)	45	1372
GC/GNR2 ($8 \mu g cm^{-2}$)	360	188
GC/GNR2 ($2 \mu g cm^{-2}$)	480	144
GC/GNR1 ($80 \mu g cm^{-2}$)	25	2065
GC/GNR1 ($32 \mu g cm^{-2}$)	60	947
GC/GNR1 ($8 \mu g cm^{-2}$)	118	595
GC/GNR1 ($2 \mu g cm^{-2}$)	59	1277

[a] k^0 (or k_{app}^0) values were obtained from R_{ct} as described in the literature.²²

In summary, the high values of k_{app}^0 obtained for GC modified with $80 \mu g cm^{-2}$ of MWCNT2 or MWCNT1, or modified with $32 \mu g cm^{-2}$ of MWCNT1, in the presence of a total 2 mM concentration of $K_3[Fe(CN)_6]/K_4[Fe(CN)_6]$ (1:1 molar ratio), can be attributed to the structure of the film formed on the GC surface and/or to some residual metal remaining from the synthesis of MWCNT2 and MWCNT1, since these materials were used as received. Because fewer oxygen-containing functional groups appear to be present in GONR2 than in GONR1 (Figure 1), k_{app}^0 is on average higher for GC modified with GONR2 than for GC modified with GONR1. The opposite behavior is observed for GNR1 relative to GNR2—i.e., k_{app}^0 is on average higher for GC modified with GNR1 (Table 1). The k_{app}^0 values obtained for GC modified with 80 or $8 \mu g cm^{-2}$ of GNR1 or GNR2 in the presence of a total 2 mM concentration of $K_3[Fe(CN)_6]/K_4[Fe(CN)_6]$ (1:1 molar ratio) are lower than for GC/CCG electrodes,²² most probably owing to differences in graphene structures.

CV and HV responses for bare GC electrode and GC electrodes modified with $80 \mu\text{g cm}^{-2}$ of MWCNT1, MWCNT2, GONR1, GONR2, GNR1, or GNR2, in 0.1 M HClO_4 , 0.1 KH_2PO_4 (pH 7.0), or 0.1 M KOH solutions saturated with N_2 or O_2

To further characterize the modified GC electrodes, the mechanism of ORR taking place on their surfaces was investigated considering that kinetic sensitivity of oxygen as a redox probe is influenced by particular modifications made to carbon electrode surfaces.^{22,42} McCreery⁴² reported that O_2 requires adsorption, is not affected by oxides, and is surface-sensitive, whereas $\text{Fe}(\text{CN})_6^{3-/4-}$ most probably does not require adsorption, is not affected by oxides, and is surface-sensitive on carbon electrodes. This warrants the use of a GC surface (carbon material) to compare its electrochemical behavior with those of other carbon nanomaterials.

Figures S9-S11 (Supporting Information) show CV readings for bare GC electrodes and GC electrodes modified with $80 \mu\text{g cm}^{-2}$ of MWCNT1, MWCNT2, GNR1, or GNR2, taken in N_2 - or O_2 -saturated 0.1 M HClO_4 (Figure S9), 0.1 M KH_2PO_4 (Figure S10), or 0.1 M KOH (Figure S11).

Throughout the scanned potential region, low currents were observed for GC/MWCNT1 and GC/MWCNT2 in the presence of N_2 -saturated 0.1 M HClO_4 and for bare GC and GC/MWCNT2 in the presence of O_2 -saturated 0.1 M HClO_4 (Figure S9, Supporting Information). However, in the presence of O_2 -saturated 0.1 M HClO_4 (Figure S9), the currents became more negative at potentials more negative than -0.34 V, further increasing in negative value in the negative-going potential scan for bare GC/MWCNT1 and GC/GNR2. At the GC/GNR1 electrode, negative currents began to increase at potentials more negative than -0.24 V (see references 43-49 for descriptions of different ORR mechanisms). In terms of potential, these findings suggest the occurrence of catalysis mediated by GC/MWCNT1, GC/GNR2, and particularly GC/GNR1 in ORR, most probably in competition with H_2 production (hydrogen bubbles were observed on these modified electrodes), relative to the other modified electrodes in acidic solution.

In the presence of N_2 -saturated 0.1 M KH_2PO_4 (pH 7.0) or 0.1 M KOH solutions (Figures S10 and S11, Supporting Information), GC/MWCNT2 and GC/MWCNT1 exhibited solely capacitive currents. In O_2 -saturated 0.1 KH_2PO_4 (pH 7.0), however, all the electrodes exhibited roughly the same peak (wave) current values, with onset potentials of 0.22 for bare GC and 0.52-0.60 V for both GC/MWCNT2 and GC/GNR1. In O_2 -saturated 0.1 M KOH, a small peak current at an onset potential of around 0.80 V was observed for GC/MWCNT1, GC/GNR2, and GC/GNR1, with approximately the same current values as the peak (or wave) observed in 0.1 M KH_2PO_4 (pH 7.0). In addition, the GC/MWCNT2 electrode showed an onset potential of 0.72 V for a sequence of poorly defined peaks with high currents (the potential for the central peak was 0.07 V), characteristic of residual metals employed in the synthesis of MWCNT2 (used as received). Bare GC showed an onset potential of 0.62 V, while GC/MWCNT1 exhibited high currents at potentials more negative than -0.40 V, characteristic of H_2 production. These onset potentials were close to that previously obtained by our group for GC/CCG electrodes²² considering the correction applied to a saturated calomel electrode (SCE, used as the reference electrode), based on an RHE.

It is assumed that the small peak observed for the 0.1 M KOH solution (as well as the peak or wave for 0.1 M HClO_4 and 0.1 KH_2PO_4 (pH 7.0)) is associated with a single-electron process—namely, $\text{O}_2 + \text{H}_2\text{O} + 2\text{e}^- \rightarrow \text{HO}_2^- + \text{OH}^-$ for alkaline solutions or $\text{O}_2 + 2\text{H}^+ + 2\text{e}^- \rightarrow \text{H}_2\text{O}_2$ for acidic solutions^{22,49} (see also references 50 and 51 for details on a proposed mechanism for ORR in alkaline solutions)—as suggested by Taylor and Humfray,⁴⁷ who claim that, at potentials less negative than roughly -1.3 V, ORR proceeds

almost exclusively to the peroxide stage, with further reduction to water becoming increasingly significant only at more negative potentials.

Figures 5-7 and Figures S12-S17 (Supporting Information) show the hydrodynamic voltammetry curves for bare or modified GC electrodes, obtained in O_2 -saturated 0.1 M HClO_4 (Figures 5 and S12-S13), 0.1 M KH_2PO_4 (pH 7.0) (Figures 6 and S14-S15), and 0.1 M KOH (Figures 7 and S16-S17), with subtraction of background hydrodynamic voltammetric curves obtained using the respective electrodes in their respective N_2 -saturated 0.1 M solutions.

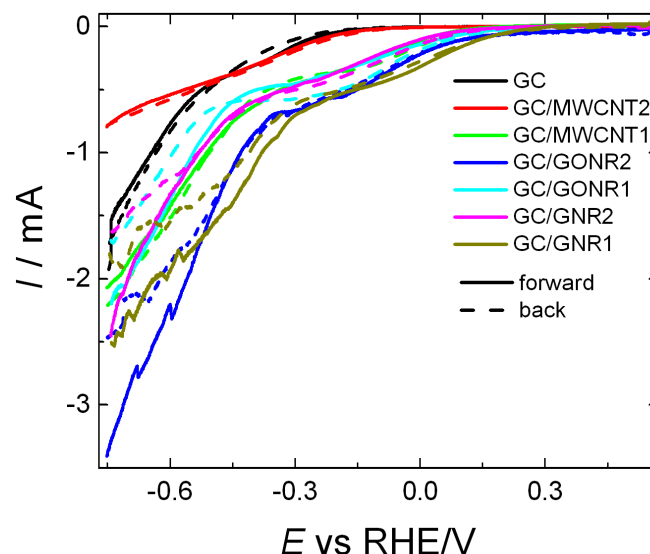


Figure 5. Hydrodynamic voltammetry curves obtained in O_2 -saturated 0.1 M HClO_4 for O_2 reduction on a bare GC electrode and GC electrodes surface-modified with $80 \mu\text{g cm}^{-2}$ of MWCNT1, MWCNT2, GONR1, GONR2, GNR1, or GNR2, subtracted from their respective hydrodynamic voltammetry curves obtained in N_2 -saturated 0.1 M HClO_4 . $\omega = 1600$ rpm; $v = 10$ mV s^{-1} . Scans started at -0.75 V.

In O_2 -saturated 0.1 M HClO_4 (Figure 5), the currents started to increase after approximately -0.28 V, with a second regime of current increase after -0.47 V in both potential scan directions for bare GC and GC/MWCNT2 electrodes. Currents were lower (on average) in the positive-going than in the negative-going scan (Figure 5). On average, GC/MWCNT1, GC/GONR1, and GC/GNR2 electrodes exhibited an onset potential of 0.10 V (Figure 5 and Figure S13, Supporting Information), in addition to much higher currents after -0.42 V in both potential scan directions. GC/GONR2 and GC/GNR1 exhibited an onset potential of around 0.18 V (Figure 5 and Figure S12, Supporting Information), in addition to much higher currents after -0.34 V in both potential scan directions, compared with bare GC, suggesting that GC/GONR2 and GC/GNR1 have a more effective catalytic behavior towards ORR, mostly owing to the more positive onset potential, since increased currents after -0.34 V would involve competition with H_2 production, precluding determination of a well-defined limit current for ORR on bare or modified GC electrodes (see Figures S12 and S13, Supporting Information, for the presence of current “noise” at potentials more negative than -0.34 V, resulting from H_2 production). For GC/GONR2 and GC/GNR1 electrodes, currents were higher (on average) during the positive-going than the negative-going scan (Figure 5). For these electrodes, the catalytic behavior towards ORR was also more effective than that previously obtained for GC/CCG²²

in terms of onset potential and currents in the potential range of 0.18 to -0.34 V.

In O_2 -saturated 0.1 M KH_2PO_4 (pH 7.0) (Figure 6), currents started to increase after 0.28 V for bare GC in the positive-going direction and 0.55 V for GC/MWCNT1, GC/MWCNT2, GC/GONR1, GC/GONR2, GC/GNR1, and GC/GNR2 in both potential scan directions, resulting in a more effective catalytic behavior towards ORR for these modified electrodes. The currents were lower (on average) during the positive-going potential scan than in the negative direction (Figure 6 and Figures S14–S15, Supporting Information), with the exception of bare GC. GC/GNR1 and GC/GNR2 electrodes showed improved current values, relative to the other modified electrodes, and higher catalytic behavior towards ORR than that previously obtained for GC/CCG²² in terms of onset potential and currents in the potential range of 0.55 to -0.30 V, considering the potential correction applied to SCE, based on HRE.

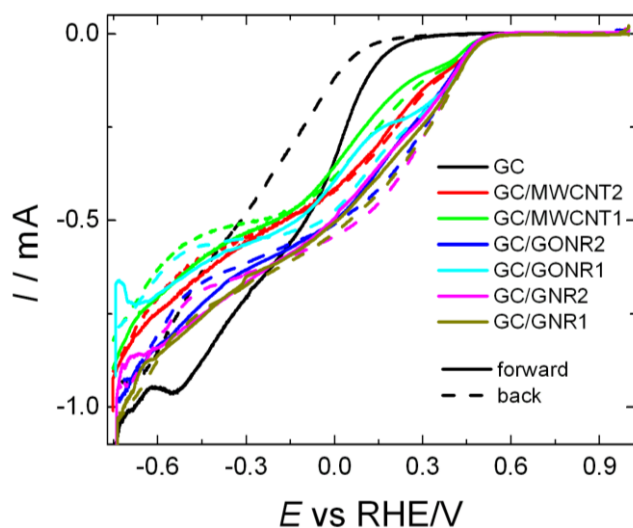


Figure 6. Hydrodynamic voltammetry curves obtained in O_2 -saturated 0.1 M KH_2PO_4 (pH 7.0) for O_2 reduction on a bare GC electrode and GC electrodes surface-modified with $80 \mu g cm^{-2}$ of MWCNT1, MWCNT2, GONR1, GONR2, GNR1, or GNR2, subtracted from their respective hydrodynamic voltammetry curves obtained in N_2 -saturated 0.1 M KH_2PO_4 (pH 7.0). $\omega = 1600$ rpm; $v = 10$ mV s^{-1} . Scans started at -0.75 V.

In O_2 -saturated 0.1 M KOH (Figure 7, which also depicts the same curves plotted in terms of current densities), currents started to increase after roughly 0.67 V for bare GC, 0.75 V for GC/MWCNT2, 0.81 V for GC/MWCNT1, GC/GONR2, GC/GONR1, and GNR2, and 0.87 V for GC/GNR1, with a peak current observed at around 0.45 V for bare GC and GC/MWCNT2 and at approximately 0.50 V for GC/GNR2, with current and peak current values at more negative potentials rising from bare GC to GC/MWCNT1 to GC/GNR1 to GC/GNR2, with a more effective catalytic behavior towards ORR for the latter two electrodes in terms of potentials and currents. Overall, currents were lower during the positive-going potential scan than in the negative direction, and clearly were limit currents for ORR (Figures 7, and S16 and S17 in the Supporting Information). The catalytic behavior of GC/GNR1 and GC/GNR2 towards ORR was more effective than that previously obtained for GC/CCG²² in terms of onset potential and currents in the potential range of 0.87 to 0.00 V, considering the potential correction applied to SCE, relative to HRE. In the present experiment, however, catalytic behavior was lower than that reported by Dai and co-workers¹⁶ for NT-G complexes acting as ORR

electrocatalysts in acidic and alkaline solutions, and lower than that reported by Yamauchi and co-workers¹ for NMCS-3 acting as ORR electrocatalysts in 0.1 M KOH. An important aspect is that the loadings of NT-G complexes ($487.2 \mu g cm^{-2}$) employed by Dai and co-workers¹⁶ and of NMCS-3 ($707 \mu g cm^{-2}$) employed by Yamauchi and co-workers¹ onto GC were six and nine times higher, respectively, than in the present study. In addition, our HV results for ORR were close to those reported by Gong *et al.*¹⁷ for VANCNT catalysts in 0.1 M KOH,^{17,18} slightly higher than that described by Yang *et al.*¹⁹ for boron-doped carbon nanotubes (loading of $102 \mu g cm^{-2}$ onto GC) in 0.1 M NaOH, close to that reported by Park *et al.*²⁰ for NRGOn (loading of $71 \mu g cm^{-2}$ onto GC) in 0.5 M KOH, and higher than the results reported by Huang *et al.*²¹ for a [PDDA@ERGO] multilayer film (of unclear loading onto GC, but of $36 \mu g cm^{-2}$ onto an ERGO/GC electrode) in 0.1 M KOH.

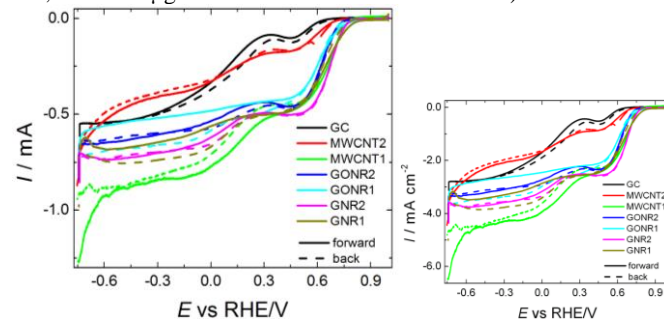


Figure 7. Hydrodynamic voltammetry curves obtained in O_2 -saturated 0.1 M KOH for O_2 reduction on a bare GC electrode and GC electrodes surface-modified with $80 \mu g cm^{-2}$ of MWCNT1, MWCNT2, GONR1, GONR2, GNR1, or GNR2, subtracted from their respective hydrodynamic voltammetry curves obtained in N_2 -saturated 0.1 M KOH. $\omega = 1600$ rpm; $v = 10$ mV s^{-1} . Scans started at -0.75 V. Note that plotting E vs. RHE values against current densities (right-hand graph) yielded the same curves. Current densities were determined by dividing the currents depicted in the left-hand graph by the geometric area of the electrode.

The peak current observed for bare GC is in agreement with our previous paper²² and with a study by Tammeveski *et al.*⁵¹ Also, the current minimum, at around 0.32 V (Figure 7), has been tentatively explained as due to a decrease in the number of electrocatalytically active surface sites for oxygen reduction.^{22,47,51} Moreover, there are indications that treatments of carbon that tend to increase coverage by quinonoid-type functional groups render the surface more active for O_2 reduction in alkaline solutions.^{51,52} Applied to GC/MWCNT2 and GC/GONR2 electrodes, the latter information is consistent with the presence of the large number of nanoribbons in the GONR2 sample (Table 1). This sample would have at its edges not only the groups proposed in Scheme 1, but also carboxyl, phenol, lactone, and quinone groups, which are primarily present at the sheet edges, and hydroxyl and epoxy groups, present on the basal plane.^{4,5,8,10,11,24} Hydrazine effectively removes in-plane functional groups such as epoxy and hydroxyl, while leaving edge moieties such as carboxyl (and not only the groups proposed in Scheme 2) intact.^{4,5,8,10,11,24} These features might explain the proximity, in shape and current values, between GC/GONR2 and GC/GNR2 hydrodynamic voltammetry curves, since the quinones located at the edge are not removed by reduction with hydrazine. Compared with MWCNT1, GONR1 exhibits disruption at the π network edge (Table 1), due to production of carboxyl, carbonyl, phenol, lactone, quinone, hydroxyl, and epoxy groups after MWCNT1 oxidation^{4,5,8,10,11,24} (in Figure 7, see the decreased currents for GC/GONR1, relative to GC/MWCNT1, with subsequent increase after hydrazine reduction of GONR1 (GC/GNR1 electrode)). GONR1 reduction by hydrazine

recovers some of the π network edges for GNR1 by removal of hydroxyl and epoxy groups from the GONR1 edge.

In interpreting hydrodynamic voltammetry responses, it is well established that deviations from a straight line intersecting the origin in an I vs. $\omega^{1/2}$ plot suggest that the electron-transfer reaction is kinetically limited.⁴⁰ Because the current responses shown in Figures S12-S17 (Supporting Information) were not linear against $\omega^{1/2}$, although the lines intersected the origin (plots not shown), Equation 1 was employed to calculate the I^{-1} vs. $\omega^{-1/2}$ (Koutecký–Levich (K-L)) plots⁴⁰ depicted in Figures S18-S26 (Supporting Information):

$$\frac{1}{I} = \frac{1}{I_k} + \frac{1}{I_d} = \frac{1}{nF(EC'SA)kC_{O_2}^b} - \frac{1}{0.62nFAD_{O_2}^{2/3}\nu^{-1/6}C_{O_2}^b\omega^{1/2}} \quad (1)$$

where I is the measured current, I_k is the kinetic current, I_d is the diffusion-limited current, k is the overall rate constant for O_2 reduction, $C_{O_2}^b$ is the bulk oxygen concentration (1.2×10^{-6} mol cm^{-3}),^{53,54} D_{O_2} is the diffusion coefficient of oxygen (1.9×10^{-5} cm^2 s^{-1}),^{53,54} ν is the kinematic viscosity of the solution (0.01 cm^2 s^{-1}),⁵⁵ and ω is the rotation rate.

Given that our K-L plots exhibited linear, parallel behavior (Figures S18-S26, Supporting Information) without intercepting the origin, the discussion of these results will be based on Equation 1. The linear behavior observed in the K-L plots in Figures S18-S26 (Supporting Information) yielded intercept values ranging from -0.09 to -23.8 mA^{-1} and slope values varying from -10.7 to -83.3 $mA^{-1} s^{-1/2}$. From the former range, it was possible to obtain k from the first contribution on the right-hand side of Equation 1, considering the n values obtained from the slope values related to the second term on the right-hand side of this equation (see Figure 8 and Figure S27, Supporting Information).

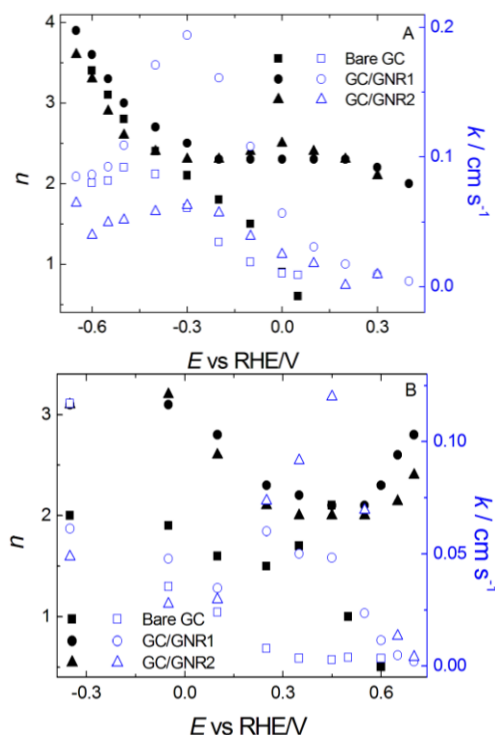


Figure 8. n and k vs. E plots obtained from data in Figures S21-S26 (Supporting Information) for O_2 reduction on a bare GC electrode and GC electrodes surface-modified with $80 \mu g cm^{-2}$ of GNR1 or GNR2, in O_2 -saturated 0.1 M KH_2PO_4 (pH 7.0) (A) and 0.1 M KOH (B).

Figure 8A reveals that n values obtained after 0.05 V in the negative-going potential scan increase almost linearly from 0.6 (reaching a value of 2 at -0.30 V) to 3.4 at -0.60 V for bare GC. For a GC electrode surface-modified with $80 \mu g cm^{-2}$ of GNR1 or GNR2, n has an average value of 2.3 within the range of 0.4 V to -0.3 V, increasing to close to 4.0 at -0.65 V in the negative-going potential scan. For k values, an increase to a maximum is evident in the negative-going direction for all electrodes, but the GC electrode modified with $80 \mu g cm^{-2}$ of GNR1 yielded a maximum k value of 0.19 $cm s^{-1}$ at -0.30 V, while at the same potential the electrode modified with $80 \mu g cm^{-2}$ of GNR2 yielded a maximum value of 0.06 $cm s^{-1}$. Bare GC yielded a maximum value of 0.09 $cm s^{-1}$ at -0.50 V. This observation closely corresponds with the potential at which O_2 reduction exhibits near-limit currents (see Figure 6 and Figures S14-S15, Supporting Information). These results revealed the enhanced catalytic behavior towards ORR exhibited by the GC electrode modified with $80 \mu g cm^{-2}$ of GNR1, compared with bare GC or GC modified with $80 \mu g cm^{-2}$ of GNR2, investigated here in 0.1 M KH_2PO_4 (pH 7.0). During ORR, similar n values and increased k values were observed for GC modified with $80 \mu g cm^{-2}$ of GNR1 or GNR2, relative to GC modified with $8.0 \mu g cm^{-2}$ of CCG,²² considering the potential correction applied to SCE, relative to HRE.

Use of a Au ring (Figure 9A) revealed that maximum production of H_2O_2 is very close to the lowest value of n and highest value of k (Figure 8A), which, at -0.30 V, results in production of only 1.45% of H_2O_2 at the GC electrode modified with $80 \mu g cm^{-2}$ of GNR1 (Table S2) in the negative-going potential scan. This electrode also produced more H_2O_2 —kinetically faster production (higher k values)—during ORR than did bare GC or GC modified with $80 \mu g cm^{-2}$ of GNR2 (Table S2) in buffered solution (pH 7.0), despite a much higher production of H_2O_2 .

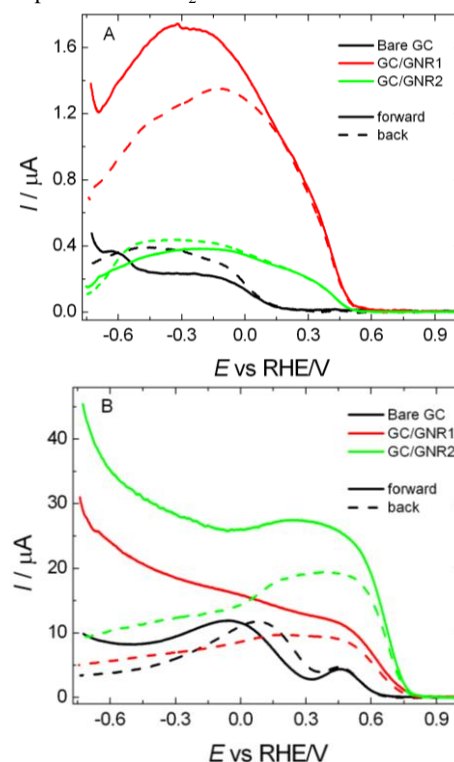


Figure 9. Hydrodynamic voltammetric curves for a Au ring electrode maintained at 1.0 V during potential scan (scan rate: 10 $mV s^{-1}$) using a bare GC disk electrode and GC disk electrodes modified with $80 \mu g cm^{-2}$ of GNR1 or GNR2, in O_2 -saturated 0.1 M KH_2PO_4 (pH 7.0) (A) and 0.1 M KOH (B). $\omega = 1600$ rpm.

In 0.1 M KOH (Figure 8B), the GC electrode modified with 80 $\mu\text{g cm}^{-2}$ of GNR1 yielded n values starting at 2.8, reaching a minimum of 2.1 at 0.45 V, and rising to 3.1 at -0.05 V in the negative-going potential scan. A similar behavior was observed for GC modified with 80 $\mu\text{g cm}^{-2}$ of GNR2—i.e., n starting at 2.4, reaching a minimum of 2.0 at 0.45 V, and rising to 3.2 at -0.05 V in the negative-going potential scan. Bare GC reached a maximum n of 2.1 at 0.45 V in the negative-going potential scan. The value of k peaked in the negative-going direction for a GC electrode modified with 80 $\mu\text{g cm}^{-2}$ of GNR2, reaching 0.12 cm s^{-1} at 0.45 V. For GC modified with 80 $\mu\text{g cm}^{-2}$ of GNR1, k peaked at 0.06 cm s^{-1} at 0.25 V in the negative-going direction; for bare GC, k peaked at 0.12 cm s^{-1} at -0.35 V in the same scan direction. This observation closely corresponds with the potential at which limit currents for O_2 reduction start (see Figure 7 and Figures S16–S17, Supporting Information). These results reveal the enhanced catalytic behavior towards ORR exhibited by the GC electrodes modified with 80 $\mu\text{g cm}^{-2}$ of GNR2, relative to bare GC or GC modified with 80 $\mu\text{g cm}^{-2}$ of GNR1, investigated here in 0.1 M KOH. During ORR, similar n values and increased k values were found for GC modified with 80 $\mu\text{g cm}^{-2}$ of GNR1 or GNR2, relative to GC modified with 8.0 $\mu\text{g cm}^{-2}$ of CCG,²² considering the potential correction applied to SCE, relative to HRE.

Maximum production of H_2O_2 (Figure 9B) was also close to the lowest value of n and the highest value of k (Figure 8B), resulting in production of 34.1% of H_2O_2 at 0.45 V and 14.1% at -0.35 V at the GC electrode modified with 80 $\mu\text{g cm}^{-2}$ of GNR2 (Table S2), in the negative-going potential scan (H_2O_2 production, of 37.4% at -0.35 V, was lower than that of 49.2% at 0.45 V obtained in the positive-going scan) (Table S2). This electrode also produced more H_2O_2 —kinetically faster production (higher k values)—during ORR than did bare GC or GC modified with 80 $\mu\text{g cm}^{-2}$ of GNR1 (Table S2) in 0.1 M KOH, although with sufficient generation of H_2O (around 50%). Our rates of H_2O_2 production were much higher than those (of roughly 3%) obtained by Dai and co-workers.¹⁶ However, high H_2O_2 production during ORR was reported by Yang *et al.*¹⁹ for boron-doped carbon nanotubes in 0.1 M NaOH and by Yamauchi and co-workers¹ for NMCS-3 in 0.1 M KOH, while Park *et al.*²⁰ observed around 30% for NRGOn in 0.5 M KOH, and Huang *et al.*²¹ reported high H_2O_2 generation for a [PDDA@ERGO] multilayer film in 0.1 M KOH.

Figure S27 (Supporting Information) shows that n increased relatively linearly in the negative-going potential direction for all electrodes in 0.1 M HClO_4 . For a GC electrode modified with 80 $\mu\text{g cm}^{-2}$ of GNR1, n starts at 1.6 at 0.1 V and reaches 4.2 at -0.35 V in the negative-going potential scan. For a GC electrode modified with 80 $\mu\text{g cm}^{-2}$ of GNR2, n starts at 1.8 at 0.05 V, reaching 2.9 at -0.35 V in the negative-going potential direction. For bare GC, n reaches a value of 2.0 at -0.40 V. The values of k increase in the negative-direction potential scan for all electrodes, reaching 0.015 cm s^{-1} at -0.15 V for GC modified with 80 $\mu\text{g cm}^{-2}$ of GNR1 and 0.026 cm s^{-1} at -0.25 V for GC modified with 80 $\mu\text{g cm}^{-2}$ of GNR2—relatively low values, if compared with those shown in Figure 8. This finding closely corresponds with the potential at which the limit currents for O_2 reduction start (see Figure 5 and Figures S12–S13, Supporting Information). These results reveal a mild enhancement of the catalytic behavior towards ORR of the GC electrodes modified with 80 $\mu\text{g cm}^{-2}$ of GNR1, relative to bare GC or GC modified with 80 $\mu\text{g cm}^{-2}$ of GNR2, studied here in 0.1 M HClO_4 . During ORR, similar n values and increased k values, observed at more positive potentials, were found for GC modified with 80 $\mu\text{g cm}^{-2}$ of GNR1 or GNR2, compared with GC modified with 8.0 $\mu\text{g cm}^{-2}$ of CCG.²²

Detection of H_2O_2 in 0.1 M HClO_4 after ORR was negligible (Table S2 and Figure S28, Supporting Information; at -0.15 V, H_2O_2

production was only 0.13% for GC modified with 80 $\mu\text{g cm}^{-2}$ of GNR1, in the negative-direction potential scan). Our rates of H_2O_2 production were lower than those (of roughly 3%) obtained by Dai and co-workers.¹⁶

The values found for n , k , and H_2O_2 percentage suggest that ORR proceeds predominantly towards H_2O ($\text{O}_2 + 4\text{H}^+ + 4\text{e}^- \rightarrow 2\text{H}_2\text{O}$), while also progressing, to a lesser degree (albeit to a very high degree in KOH, approaching 50% of H_2O_2 production), to the peroxide stage ($\text{O}_2 + 2\text{H}^+ + 2\text{e}^- \rightarrow \text{H}_2\text{O}_2$), which can be followed by H_2O production as per $\text{H}_2\text{O}_2 + 2\text{H}^+ + 2\text{e}^- \rightarrow \text{H}_2\text{O}$.⁴⁹ Parallel mechanisms—i.e., both four- and two-electron reductions—have been reported for strongly acidic media, and possibly for high-surface-area carbons in alkaline electrolytes.⁴⁴

Table 2 summarizes the Tafel slopes obtained from Figures S29–S31 (Supporting Information) for ORR taking place on bare and modified GC surfaces in different solutions.

Table 2. Tafel slopes obtained from Figures S29–S31 (Supporting Information) for ORR on bare and modified GC electrode surfaces.

Solution	Electrode (and modifier loading)	Low polarization (low currents) (mV decade ⁻¹)	High polarization (high currents) (mV decade ⁻¹)
0.1 M HClO_4	Bare GC	–161	–78
	GC/GNR1 (80 $\mu\text{g cm}^{-2}$)	–170	–157
	GC/GNR2 (80 $\mu\text{g cm}^{-2}$)	–150	–210
0.1 M KH_2PO_4 (pH 7.0)	Bare GC	–194	–143
	GC/GNR1 (80 $\mu\text{g cm}^{-2}$)	–77	–270
	GC/GNR2 (80 $\mu\text{g cm}^{-2}$)	–83	–120
0.1 M KOH	Bare GC	–127	–250
	GC/GNR1 (80 $\mu\text{g cm}^{-2}$)	–146	–251
	GC/GNR2 (80 $\mu\text{g cm}^{-2}$)	–88	–142

In the presence of 0.1 M HClO_4 , Tafel slopes under low polarization are close to -160 mV decade⁻¹, irrespective of electrode. Under high polarization, however, Tafel slopes increase from -78 mV decade⁻¹ for bare GC to -210 mV decade⁻¹ for GC modified with 80 $\mu\text{g cm}^{-2}$ of GNR2 (Table 2). The values obtained under high polarization for GC modified with 80 $\mu\text{g cm}^{-2}$ of GNR1 or GNR2 are akin to those reported by Tarasevich *et al.*⁴⁴ (from -0.14 to -0.17 V decade⁻¹ under high polarization for ORR on pyrolytic GR in acidic solution). This lends credence to the assumption that changes in Tafel slopes for different surfaces are most likely related to different steps occurring or prevailing on these surfaces during ORR. Our Tafel slopes are higher than those (of roughly -68 mV decade⁻¹) reported by Dai and co-workers.¹⁶

In buffered solution (0.1 M KH_2PO_4 , pH 7.0), high Tafel slopes, of around -194 mV decade⁻¹ for bare GC, were detected under low polarization, which decreased to nearly 80 mV decade⁻¹ for GC modified with 80 $\mu\text{g cm}^{-2}$ of GNR1 or GNR2, while under high polarization the slopes decreased from -143 mV decade⁻¹ for bare GC to -120 mV decade⁻¹ for GC modified with 80 $\mu\text{g cm}^{-2}$ of GNR2 (Table 2), and even increased (-270 mV decade⁻¹) for GC modified with 80 $\mu\text{g cm}^{-2}$ of GNR1. A similar behavior was found in alkaline solutions, with Tafel slopes for 0.1 M KOH decreasing from -136 (on average) to -88 mV decade⁻¹ under low polarization, and from -250 to -142 mV decade⁻¹ for GC modified with 80 $\mu\text{g cm}^{-2}$ of

GNR2 under high polarization (Table 2). On average, these results are in agreement with the literature, bearing direct relation to electrode surface and to complex ORR mechanisms involved on each surface, as can be inferred from the study of pyrolytic GR in alkaline electrolytes conducted by Tarasevich *et al.*,⁴⁴ who reported two distinct cathodic Tafel slopes, of around $-0.03 \text{ V decade}^{-1}$ under low polarization and ranging from -0.08 to $-0.14 \text{ V decade}^{-1}$ under high polarization. By contrast, Yeager *et al.*,⁴⁵ having found one single Tafel slope, ranging from -0.12 to $-0.15 \text{ V decade}^{-1}$, while investigating various GR and carbon electrodes, suggested that this behavior is related to a rate-determining one-electron transfer step with a nearly symmetrical potential-energy barrier. Morcos and Yeager⁴⁶ found that ordinary and high-pressure-annealed pyrolytic GR had Tafel slopes of $-0.11 \text{ V decade}^{-1}$, while the cleavage surface of high-pressure-annealed pyrolytic GR had a Tafel slope of $-0.10 \text{ V decade}^{-1}$. On the cleavage surface of single-crystal GR and high-pressure-annealed pyrolytic GR, ORR proceeds far slower than on the edge orientation of high-pressure-annealed pyrolytic GR or on the cleavage surface of ordinary GR.⁴⁵ Taylor and Humffray⁴⁷ found Tafel slopes close to $-0.060 \text{ V decade}^{-1}$ for ORR on a bare GC electrode in 0.1 M NaOH at low potentials, whereas at more negative potentials (high polarization) the slopes increased from -0.090 to $-0.12 \text{ V decade}^{-1}$. Yeager^{48,49} pointed out that mechanistic differences appear to exist between ORR occurring on ordinary pyrolytic GR surfaces and GC—*i.e.*, on the former, a Tafel slope of $-0.12 \text{ V decade}^{-1}$ was reported for alkaline electrolytes, with a stoichiometric number of 2 for the overall two-electron reduction of O_2 to HO_2^- , while for GC a Tafel slope of $-0.06 \text{ V decade}^{-1}$ was reported, with a stoichiometric number of 1 for the reaction $\text{O}_2 + \text{H}_2\text{O} + 2\text{e}^- \rightarrow \text{HO}_2^- + \text{OH}^-$. For both surfaces, ORR is first-order in O_2 . Also, our Tafel slope results for GC modified with $80 \mu\text{g cm}^{-2}$ of GNR2 proved very similar to our previously published values obtained for a GC electrode modified with $8.0 \mu\text{g cm}^{-2}$ of CCG,²² particularly in the case of buffered and 0.1 M KOH solutions.

In summary, the present results suggest the occurrence of catalysis, given the higher potential and average current values obtained for ORR at GC/GNR1 and GNR2 electrodes, relative to other modified electrodes, in acidic, $0.1 \text{ M KH}_2\text{PO}_4$ (pH 7.0), and 0.1 M KOH solutions. The average value of n for GC modified with $80 \mu\text{g cm}^{-2}$ of GNR1 or GNR2 was 2.3, rising to around 4.0 at -0.66 V in the negative-going potential scan in $0.1 \text{ M KH}_2\text{PO}_4$ (pH 7.0). Concomitantly, k increased to a maximum of 0.19 cm s^{-1} at -0.30 V for GC modified with $80 \mu\text{g cm}^{-2}$ of GNR1. The values obtained for n , k , and H_2O_2 percentage suggest that ORR proceeded predominantly to H_2O ($\text{O}_2 + 4\text{H}^+ + 4\text{e}^- \rightarrow 2\text{H}_2\text{O}$) and, to a lesser degree, to the peroxide stage ($\text{O}_2 + 2\text{H}^+ + 2\text{e}^- \rightarrow \text{H}_2\text{O}_2$), which could be followed by H_2O production ($\text{H}_2\text{O}_2 + 2\text{H}^+ + 2\text{e}^- \rightarrow \text{H}_2\text{O}$), both in acidic and buffered solutions. In alkaline media, n values for GC modified with $80 \mu\text{g cm}^{-2}$ of GNR1 or GNR2 started at 2.6 on average, reaching a minimum of 2.0 at 0.45 V and rising to around 3.1 at -0.05 V in the negative-going potential scan. The values of k peaked in the negative-going potential scan for all electrodes, yet GC modified with $80 \mu\text{g cm}^{-2}$ of GNR2 yielded a k value of 0.12 cm s^{-1} at 0.45 V . This GC-modified electrode produced H_2O_2 substantially, at up to 50%—kinetically faster production (higher k values)—during ORR. Also, the different surfaces investigated yielded different Tafel slopes for ORR, most probably because different steps (reactions) take place or prevail during ORR on these surfaces in different media.

Conclusions

GONRs were synthesized from MWCNTs by way of a pre-oxidation step with peroxydisulfate involving phosphorus pentoxide ester formation and proceeding to oxidation with permanganate. GONRs reductions to yield GNRs were conducted with hydrazine. In the

synthesized GONRs, hollow walls were absent and the carbon nanostructures were in the 20 nm range. GNR1 resembles an internodal segment of bamboo cut lengthwise, with a shallow troughing at its center, while GNR2 resembles stacked ribbons, each $\sim 16 \text{ nm}$ wide, with points of structural damage and points of four-ribbon connection measuring 60 nm or wider. The combination of CV and EIS data obtained with the modified electrodes revealed that GC coated with GNR1 in the presence of a total 2 mM concentration of $\text{K}_3[\text{Fe}(\text{CN})_6]/\text{K}_4[\text{Fe}(\text{CN})_6]$ (1:1 molar ratio) exhibited a high charge-transfer rate (k_{app}^0). High ECSA values were found for GC surface-modified with GNR1 and GNR2. The GC/GNR1 and GC/GNR2 electrodes proved sufficiently catalytic towards ORR, compared with the other modified electrodes investigated in acidic, $0.1 \text{ M KH}_2\text{PO}_4$ (pH 7.0), and 0.1 M KOH solutions (HV results). In GC modified with $80 \mu\text{g cm}^{-2}$ of GNR1 or GNR2, n ranged from 2.3 to 4.0, while k reached 0.19 cm s^{-1} , with only 1.45% of H_2O_2 production in $0.1 \text{ M KH}_2\text{PO}_4$ (pH 7.0). The values obtained for n , k , and H_2O_2 percentage suggest that ORR predominantly proceeded to H_2O ($\text{O}_2 + 4\text{H}^+ + 4\text{e}^- \rightarrow 2\text{H}_2\text{O}$) and, to a lesser degree, to the peroxide stage ($\text{O}_2 + 2\text{H}^+ + 2\text{e}^- \rightarrow \text{H}_2\text{O}_2$), which could be followed by H_2O production ($\text{H}_2\text{O}_2 + 2\text{H}^+ + 2\text{e}^- \rightarrow \text{H}_2\text{O}$), both in acidic and buffered solutions. In alkaline media, n values for GC modified with $80 \mu\text{g cm}^{-2}$ of GNR1 or GNR2 ranged from 2.6 to 3.1, while k reached 0.12 cm s^{-1} , with high production of H_2O_2 (*e.g.*, 50%)—kinetically faster production, coincident with high k values—during ORR. The various surfaces and structures exhibited by GONRs and GNRs yielded different Tafel slopes for ORR, most probably because different steps (reactions) take place or prevail during ORR on these surfaces.

Experimental Section

Reagents and instruments

$\text{K}_3[\text{Fe}(\text{CN})_6]$, $\text{K}_4[\text{Fe}(\text{CN})_6]$, H_2SO_4 , $\text{K}_2\text{S}_2\text{O}_8$, P_2O_5 , H_2O_2 , KOH , KH_2PO_4 , and ammonium hydroxide solution (28 wt% in water) (all Vetec), NaNO_3 (Merck), HCl (Merck), KMnO_4 (Nuclear), hydrazine sulfate (Dinâmica), and HClO_4 (Tedia) were all used as received. MWCNTs— $6\text{--}9 \text{ nm} \times 5 \mu\text{m}$ (O.D. \times L), 3-6 tubes (now designated MWCNT1), and $10 \pm 1 \text{ nm} \times 4.5 \pm 0.5 \text{ nm} \times 3\text{--}6 \mu\text{m}$ (O.D. \times I.D. \times L), 6-8 tubes (now termed MWCNT2)—were from Aldrich and used as received.

Voltammetric measurements were carried out using a three-electrode glass cell with a working electrode consisting of a Teflon-embedded GC disk/Au ring rotating assembly (0.196 and 0.11 cm^2 geometric areas, respectively) (Pine Research Instrumentation), with a collection efficiency of $N = 0.26$. The counter-electrode was a Pt plate (Degussa). A reversible hydrogen electrode (RHE) was employed as the reference electrode.

Electrode preparation

The working GC disk electrode was sequentially polished with 2500-grit emery paper and alumina slurries (1 and $0.05 \mu\text{m}$) and finally cleaned by sonication in Milli-Q water (Millipore), acetone, and 0.1 M HClO_4 (Tedia) solution for 5 min in each solvent. The Au ring underwent 200 cycles at 900 mV s^{-1} in the potential range of 0.05 to 1.7 V (changing the solution whenever necessary to ensure a clean surface finish). The GC disk electrode was subsequently washed with Milli-Q water, its surface dried with a N_2 flux, and a uniform thin film was produced by dripping $32 \mu\text{L}$ of a 0.5 mg mL^{-1} aqueous solution of MWCNTs, GONRs, and GNRs (loading: $80 \mu\text{g cm}^{-2}$; or with further dilution in water for loadings of 32, 8, and $2 \mu\text{g cm}^{-2}$) onto a GC disk surface and allowed to dry at room temperature. Each modified electrode was placed in an electrochemical cell containing a 0.1 M aqueous solution of HClO_4 , a 0.1 M aqueous solution of KH_2PO_4 , or an aqueous solution of KOH . The KH_2PO_4 solution was adjusted to pH 7.0 with 1 M KOH . The solutions were prepared with Milli-Q water and purged for 30

min with pure nitrogen or oxygen (Air Liquide) prior to each experiment.

Sample preparation for TEM measurements

For the TEM experiments, diluted MWCNT, GONR, or GNR aqueous solutions were dripped onto an ultrathin carbon film supported by a lacey carbon film on a 400-mesh copper grid (Ted Pella).

Apparatuses and measurements

An Autolab potentiostat/galvanostat (model PGSTAT128N) equipped with a FRA2.X module was used in EIS and other electrochemical experiments. For hydrodynamic voltammetry, an AFCBP1 bipotentiostat coupled to an AFMSRX speed controller (both from Pine Research Instrumentation) was employed. The EIS experiments were conducted at a fixed potential—namely, at an open-circuit potential (OCP) of around 0.19 V (on average) in the presence of $\text{Fe}(\text{CN})_6^{3-}/\text{Fe}(\text{CN})_6^{4-}$, with potential perturbation of 25 mV (rms) within a frequency range of 10 mHz to 100 kHz. Care was taken to ensure that AC impedance data corresponded to the interfaces being investigated at high frequencies—namely, the potentiostat employed had faster performance; the highest cut-off frequency was limited to 160 kHz for the FRA2 module, which used a fixed filter when the frequency applied exceeded 19 kHz; cables were short and, akin to the connections, were shielded; the electrochemical cell was placed inside a Faraday cage; the working electrode was positioned in front of and close to a larger Pt plate; and the SCE was placed near the working electrode. Nova 1.7 Autolab (2009) software was used to simulate the behavior of equivalent circuits of the interface in the presence of different redox probes, and the parameters of these circuits were fitted to the measured spectra using a non-linear least-squares program.

MWCNT, GONR, and GNR nanostructures were characterized by TEM, performed on a Tecnai G² apparatus (FEI) operating at 200 kV or a Philips CM200 apparatus operating at 200 kV.

TG characterizations of MWCNTs, GONRs, and GNRs were performed using a Q50 thermogravimetric analyzer (TA Instruments) on samples of 4 to 6 mg, under a N₂ gas flow (60 mL min⁻¹), at temperatures ranging from ambient to 900 °C and a heating rate of 10 °C min⁻¹, employing Pt crucibles.

ECSA (electrochemically active surface area) values (Supporting Information, Table S1) for bare GC and GC electrodes modified with MWCNT or GONR or GNR films were determined as described by Lima et al.²² Briefly, cyclic voltammograms responses for bare GC and GC electrodes modified with MWCNT or GONR or GNR films in a N₂-saturated 0.1 M KCl solution containing a total 2 mM concentration of $\text{K}_3[\text{Fe}(\text{CN})_6]/\text{K}_4[\text{Fe}(\text{CN})_6]$ (1:1 molar ratio) were used to determine the ECSA values of these electrodes.

GONR synthesis

GONRs²³ were synthesized from MWCNT1 or MWCNT2 using a modified^{22,56} Hummers and Offeman method,⁵⁷ as originally proposed by Kovtyukhova *et al.*⁵⁸ MWCNT1 (0.50 g) or MWCNT2 (0.50 g) were added to a mixture of concentrated H₂SO₄ (40 mL), K₂S₂O₈ (0.28 g), and P₂O₅ (0.29 g). The solution was heated to 80 °C using a hotplate and kept under stirring for 8 h employing a magnetic stirrer. Successively, the solution was cooled to room temperature and 100 mL of Milli-Q water was added. The product was obtained by filtering through 0.22 µm nylon film and washing with Milli-Q water to remove the residual acid until a neutral pH was achieved. The product was dried at room temperature.

Pre-oxidized MWCNT1 and MWCNT2 were then re-oxidized employing the Hummers and Offeman method,⁵⁷ as follows: 0.50 g of the desired compound was added to cold (0 °C) concentrated H₂SO₄ (40 mL) containing NaNO₃ (0.70 g). KMnO₄ (1.51 g) was then gradually added under stirring and the temperature of the mixture was kept below 20 °C in an ice bath. Successively, the

mixture was heated at 35 °C using a hotplate and kept under stirring for 2 h 30 min employing a magnetic stirrer and then slowly diluted with Milli-Q water (120 mL), keeping the temperature below 50 °C. Subsequently, the hotplate was switched off and 60 mL of Milli-Q water was added under stirring, followed by dilution with 220 mL of Milli-Q water. At this point, the mixture was brownish grey. Shortly after it reached room temperature, 40 mL of 30% H₂O₂ was added dropwise to the mixture under magnetic stirring, and the color of the mixture changed to a bright yellow, along with bubbling. The mixture was then diluted with the addition of 3.5 L of cold Milli-Q water and allowed to stand overnight, after which the supernatant was removed. The precipitate was centrifuged at 7500 rpm and washed once with Milli-Q water. The undried precipitate was then washed with 300 mL of an aqueous solution of HCl (1:10, v/v) to remove metal ions, followed by three washes with Milli-Q water in excess to remove the acid while centrifuging at 7500 rpm. The product was obtained by filtering through 0.22 µm nylon film and then washed with Milli-Q water to remove the residual acid until a neutral pH was obtained. The product was dried at room temperature. The resulting solid was air-dried and diluted to produce a MWCNT1 oxide or MWCNT2 oxide dispersion (5% w/w) by ultrasonication. Exfoliation of MWCNT1 oxide or MWCNT2 oxide⁵⁹ to GONR1 or GONR2, respectively, was achieved by ultrasonication of the dispersion for 2 h. The average yields of GONR1 and GONR2 after five repeated synthesis runs were 86 and 74 wt%, respectively.

GNR synthesis

GNR1 and GNR2^{22,23} were synthesized employing the method proposed by Li *et al.*⁵⁹ The resulting 5.0 mL homogeneous dispersion of GONR1 or GONR2 (5% w/w) was mixed with 5.0 mL of aqueous hydrazine sulfate solution (21 mg) and 35.0 µL of ammonium hydroxide solution (28 wt% in water) in a 20 mL glass vial. After being vigorously shaken for a few minutes, the vial was placed in a water bath (~95 °C) for 2 h 30 min. Upon reaching room temperature, the mixture was black. GNR1 and GNR2 were obtained after filtration under vacuum through 0.22 µm nylon film and then washed with 0.5% v/v ammonium hydroxide solution (100 mL). Excess ammonium hydroxide was removed by washing with Milli-Q water until a neutral pH was achieved. GNR1 and GNR2 thus obtained were dried under vacuum at room temperature. The average yields of GNR1 and GNR2 after five repeated synthesis runs were 93 and 83 wt%, respectively.

Acknowledgments

The authors thank CNPq (grants 301403/2011-2, 473991/2012-8, 405695/2013-6, and 442268/2014-9) and Fundect-MS (grants 23/200.583/2012, 23/200.735/2012, and 23/200.246/2014) for their financial support. F.L. thanks CAPES for the fellowships. Thanks are also given to CETENE and LME-IQ-UNESP for the TEM facilities.

Notes and references

Institute of Chemistry, Universidade Federal de Mato Grosso do Sul; Av. Senador Filinto Muller, 1555; Campo Grande, MS 79074-460, Brazil. Fax: +55 67 3345 3552; Tel: +5567 3345 3551; E-mails: fabio.lima@ufms.br; gilberto.maia@ufms.br

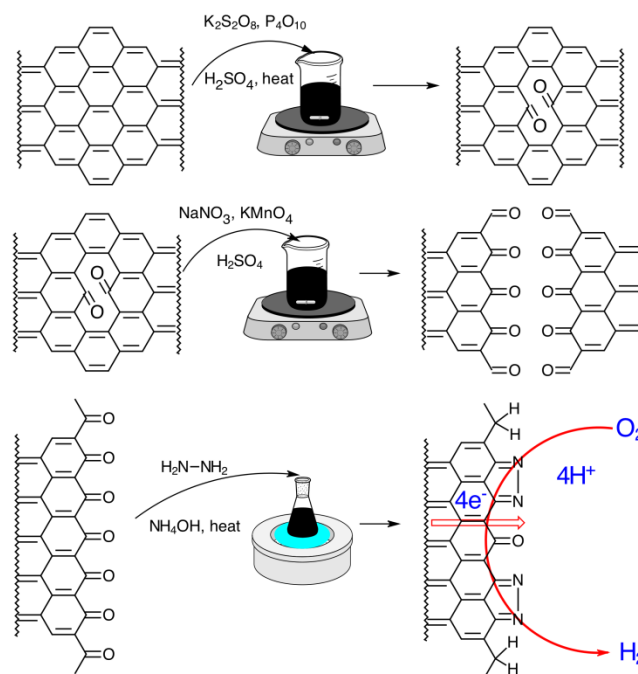
†Electronic Supplementary Information (ESI) available: The supporting information contains figures, equations, discussion, and tables concerning supplementary results, and references. See DOI: 10.1039/b000000x/

1 J. Tang, J. Liu, C. Li, Y. Li, M. O. Tade, S. Dai, and Y. Yamauchi, *Angew. Chem. Int. Ed.*, 2015, **54**, 588.

2 J. Tang, N. L. Torad, R. R. Salunkhe, J.-H. Yoon, M. S. A. Hossain, S. X. Dou, J. H. Kim, T. Kimura, and Y. Yamauchi, *Chem. Asian J.*, 2014, **9**, 3238.

- 3 J. Tang, J. Liu, N. L. Torad, T. Kimura, and Y. Yamauchi, *Nano Today*, 2014, **9**, 305.
- 4 D. V. Kosynkin, A. L. Higginbotham, A. Sinitskii, J. R. Lomeda, A. Dimiev, B. K. Price and J. M. Tour, *Nature*, 2009, **458**, 872.
- 5 A. L. Higginbotham, D. V. Kosynkin, A. Sinitskii, Z. Sun and J. M. Tour, *ACS Nano*, 2010, **4**, 2059.
- 6 J.-L. Li, K. N. Kudin, M. J. McAllister, R. K. Prud'homme, I. A. Aksay and R. Car, *Phys. Rev. Lett.*, 2006, **96**, 176101:1.
- 7 P. M. Ajayan and B. I. Yakobson, *Nature*, 2006, **441**, 818.
- 8 M. Terrones, *ACS Nano*, 2010, **4**, 1775.
- 9 N. L. Rangel, J. C. Sotelo and J. M. Seminario, *J. Chem. Phys.*, 2009, **131**, 031105:1.
- 10 D. K. James and J. M. Tour, *Acc. Chem. Res.*, 2013, **46**, 2307.
- 11 M. Terrones, *Nature*, 2009, **458**, 845.
- 12 L. Jiao, L. Zhang, X. Wang, G. Diankov and H. Dai, *Nature*, 2009, **458**, 877.
- 13 L. Jiao, X. Wang, G. Diankov, H. Wang and H. Dai, *Nat. Nanotechnol.*, 2010, **5**, 321.
- 14 L. Xie, H. Wang, C. Jin, X. Wang, L. Jiao, K. Suenaga and H. Dai, *J. Am. Chem. Soc.*, 2011, **133**, 10394.
- 15 X. Li, X. Wang, L. Zhang, S. Lee and H. Dai, *Science*, 2008, **2**, 1229.
- 16 Y. Li, W. Zhou, H. Wang, L. Xie, Y. Liang, F. Wei, J.-C. Idrobo, S. J. Pennycook and H. Dai, *Nat. Nanotechnol.*, 2012, **7**, 394.
- 17 K. Gong, F. Du, Z. Xia, M. Durstock and L. Dai, *Science*, 2009, **323**, 760.
- 18 L. Dai, D. W. Chang, J.-B. Baek and W. Lu, *Small*, 2012, **8**, 1130.
- 19 L. Yang, S. Jiang, Y. Zhao, L. Zhu, S. Chen, X. Wang, Q. Wu, J. Ma, Y. Ma and Z. Hu, *Angew. Chem. Int. Ed.*, 2011, **50**, 7132.
- 20 M. Park, T. Lee and B.-S. Kim, *Nanoscale*, 2013, **5**, 12255.
- 21 D. Huang, B. Zhang, Y. Zhang, F. Zhan, X. Xu, Y. Shen and M. Wang, *J. Mater. Chem. A*, 2013, **1**, 1415.
- 22 F. Lima, G. V. Fortunato and G. Maia, *RSC Adv.*, 2013, **3**, 9550.
- 23 G. V. Fortunato, F. Lima and G. Maia, *Nanoscale*, submitted.
- 24 R. C.-Silva, A. M.-Gómez, S. V.-Díaz, F. T.-López, A. L. Elias, N. P.-López, H. Muramatsu, T. Hayashi, K. Fujisawa, Y. A. Kim, M. Endo and M. Terrones, *ACS Nano*, 2013, **7**, 2192.
- 25 J. C. Meyer, A. K. Geim, M. I. Katsnelson, K. S. Novoselov, T. J. Booth, and S. Roth, *Nature*, 2007, **446**, 60.
- 26 J. I. Paredes, S. Villar-Rodil, P. Solís-Fernández, A. Martínez-Alonso and J. M. D. Tascón, *Langmuir*, 2009, **25**, 5957.
- 27 S. Stankovich, D. A. Dikin, R. D. Piner, K. A. Kohlhaas, A. Kleinhammes, Y. Jia, Y. Wu, S. B. T. Nguyen and R. S. Ruoff, *Carbon*, 2007, **45**, 1558.
- 28 I. K. Moon, J. Lee, R. S. Ruoff and H. Lee, *Nat. Commun.*, 2010, **1**, doi:10.1038/ncomms1067.
- 29 D. C. Marcano, D. V. Kosynkin, J. M. Berlin, A. Sinitskii, Z. Sun, A. Slesarev, L. B. Alemany, W. Lu and J. M. Tour, *ACS Nano*, 2010, **4**, 4806.
- 30 A. Citterio, C. Arnoldi, C. Giordano and G. Castaldi, *J. Chem. Soc. Perkin Trans. I*, 1983, 891.
- 31 S. Wolfe, C. F. Ingold and R. U. Lemieux, *J. Am. Chem. Soc.*, 1981, **103**, 938.
- 32 S. Park, Y. Hu, J. O. Hwang, E.-S. Lee, L. B. Casabianca, W. Cai, J. R. Potts, H.-W. Ha, S. Chen, J. Oh, S. O. Kim, Y.-H. Kim, Y. Ishii and R. S. Ruoff, *Nat. Commun.*, 2012, **3**, 638, doi: 10.1038/ncomms1643.
- 33 J. E. McMurry, *Organic Chemistry*, 6th ed., Thomson-Brooks/Cole, Belmont, CA, 2004.
- 34 R. T. Morrison and R. N. Boyd, *Organic Chemistry*, 6th ed., Prentice-Hall Inc., New Jersey, 1992.
- 35 J. A. Joule, K. Mills and G. F. Smith, *Heterocyclic Chemistry*, 3rd ed., Chapman & Hall, New York, 1995.
- 36 X. Li, T. Zhao, K. Wang, Y. Yang, J. Wei, F. Kang, D. Wu and H. Zhu, *Langmuir*, 2011, **27**, 12164.
- 37 X. Du, P. Guo, H. Song and X. Chen, *Electrochim. Acta*, 2010, **55**, 4812.
- 38 J. R. Miller, R. A. Outlaw and B. C. Holloway, *Science*, 2010, **329**, 1637.
- 39 K. Sheng, Y. Sun, C. Li, W. Yuan and G. Shi, *Sci. Rep.*, 2012, **2**, 247, doi: 10.1038/srep00247.
- 40 A. J. Bard and L. R. Faulkner, *Electrochemical Methods: Fundamentals and Applications*, 2nd ed., John Wiley & Sons, New York, 2001.
- 41 S. Krause, in *Encyclopedia of Electrochemistry*, (Eds. A. J. Bard, M. Stratmann and P. R. Unwin), Wiley-VCH, Weinheim, 2003, Vol. 3, Chapter. 2.6, pp. 196-229.
- 42 R. L. McCreery, *Chem. Rev.*, 2008, **108**, 2646.
- 43 K. Kinoshita, in *Electrochemical Oxygen Technology*, John Wiley & Sons, New York, 1992, chapter 2, pp. 19-112.
- 44 M. R. Tarasevich, A. Sadkowsky and E. Yeager, in *Comprehensive Treatise of Electrochemistry*, (Eds. B. E. Conway, J. O. M. Bockris, E. Yeager, S. U. M. Khan and R. E. White), Plenum Press, New York, 1983, Vol. 7, Chapter. 6, pp. 301-398.
- 45 E. Yeager, P. Krouse and K. V. Rao, *Electrochim. Acta*, 1964, **9**, 1057.
- 46 I. Morcos and E. Yeager, *Electrochim. Acta*, 1970, **15**, 953.
- 47 R. J. Taylor and A. A. Humffray, *J. Electroanal. Chem.*, 1975, **64**, 63.
- 48 E. Yeager, *Electrochim. Acta*, 1984, **29**, 1527.
- 49 E. Yeager, *J. Mol. Catal.*, 1986, **38**, 5.
- 50 J. Xu, W. Huang and R. L. McCreery, *J. Electroanal. Chem.*, 1996, **410**, 235.
- 51 K. Tammeveski, K. Kontturi, R. J. Nichols, R. J. Potter and D. J. Schiffrin, *J. Electroanal. Chem.*, 2001, **515**, 101.
- 52 M. S. Hossain, D. Tryk and E. Yeager, *Electrochim. Acta*, 1989, **34**, 1733.
- 53 R. E. Davis, G. L. Horvath and C. W. Tobias, *Electrochim. Acta*, 1967, **12**, 287.
- 54 R. R. Adžić, J. Wang and B. M. Ocko, *Electrochim. Acta*, 1995, **40**, 83.
- 55 CRC Handbook of Chemistry and Physics, (Ed. D. R. Lide), CRC Press, Boca Raton, 82nd ed., 2001.
- 56 Y. Xu, H. Bai, G. Lu, C. Li and G. Shi, *J. Am. Chem. Soc.*, 2008, **130**, 5856.
- 57 W. S. Hummers Jr. and R. E. Offeman, *J. Am. Chem. Soc.*, 1958, **80**, 1339.
- 58 N. I. Kovtyukhova, P. J. Ollivier, B. R. Martin, T. E. Mallouk, S. A. Chizhik, E. V. Buzaneva and A. D. Gorchinskiy, *Chem. Mater.*, 1999, **11**, 771.
- 59 D. Li, M. B. Müller, S. Gilje, R. B. Kaner and G. G. Wallace, *Nat. Nanotechnol.* 2008, **3**, 101.

Brief Abstract



GONRs were synthesized by pre-oxidizing MWCNTs with peroxydisulfate, followed by additional oxidation with permanganate and reduction with hydrazine to yield GONRs, which proved sufficiently catalytic towards ORR.